ASIM, T., MISHRA, R., OLIVEIRA, A. and CHARLTON, M. 2019. Effects of the geometrical features of flow paths on the flow capacity of a control valve trim. *Journal of petroleum science and engineering* [online], 172, pages 124-138. Available from: https://doi.org/10.1016/j.petrol.2018.09.050

Effects of the geometrical features of flow paths on the flow capacity of a control valve trim.

ASIM, T., MISHRA, R., OLIVEIRA, A. and CHARLTON, M.

2019

Effects of the Geometrical Features of Flow Paths on the Flow Capacity of a Control Valve Trim

Taimoor Asim[1*], Rakesh Mishra[2], Antonio Oliveira[3], Matthew Charlton[4]
[1,2,3] School of Computing & Engineering
University of Huddersfield, Queensgate, Huddersfield HD1 3DH, UK
[4] Weir Valves & Controls UK Ltd, Britannia House, Elland HX5 9JR, UK
[1]t.asim@hud.ac.uk, [2]r.mishra@hud.ac.uk, [3]Antonio.Oliveira2@hud.ac.uk,
[4]Matthew.Charlton@weirgroup.com

Abstract

Control valves are an integral part of a number of energy systems, such as those used in chemical and nuclear industries. These valves are used to regulate the amount of fluid flow passing through these systems. A key component of a control valve is its trim, which in case of a multi-stage continuous-resistance trim consists of a staggered arrangement of columns. Flow passing through the channels formed between adjacent columns (also called as flow paths), loses a significant amount of its energy and regulates the pressure field. As the geometrical features of these flow paths dictate the flow capacity of the trim, systematic investigations have been carried out to analyse the complex flow behaviour within these flow paths. Well-verified computational fluid dynamics based solver has been used to investigate the effects of the geometrical features of flow paths on the flow capacity of the trim, at various valve opening positions. It has been noticed that reducing the size of flow paths increases the flow capacity of the trim, however, at a critical flow path size, the inherent opening characteristics of a trim have been observed to alter. In order to recover the original opening behaviour of the trim, careful manipulation of the flow paths is required, which has been successfully achieved in the present investigation.

Keywords: Continuous-Resistance Trim, Control Valve, Computational Fluid Dynamics, Flow Capacity, Valve Opening Position

1.0 Introduction

Control valves are used worldwide in a wide range of industrial applications, including safety critical and severe service applications. There are different types of control valves, and one of the most commonly used is known as globe type control valve. The function of a control valve is to regulate the amount of fluid flow passing through it. The flow regulatory component of a control valve is its trim. There are commonly two types of trims used in globe type control valves i.e. discrete and continuous-resistance. A continuous-resistance trim comprises of a geometrically complex arrangement of columns strategically placed to create complex flow field. Conventionally, these columns are cylindrical shaped. The channels formed between adjacent columns are called flow paths. Flow passing through these flow paths loses its energy and a regulated pressure field is maintained. In a multi-stage trim, strategically placed flow paths enable the reduction in fluid pressure in a series of steps, hence, regulating the overall flow characteristics. Another important feature of a multi-stage continuous-resistance trim is its inherent opening characteristic. A multi-stage continuous-

[*] Corresponding Author
Tel.: +44 1484 472323

resistance trim can be generally one of the following types; linear opening, quick opening or equal percentage opening.

Control valves are installed in pipelines to control the process parameters corresponding to the flow of fluid passing through the flow handling system. As the control valve considered in the present study is a globe type control valve, the discussions hereafter are restricted to these valves only. A control valve primarily consists of three components. These components are the valve body, a seat and a trim, as shown in figure 1. The trim sits on top of the seat, while a plug controls the Valve Opening Position (VOP). The trim comprises of a number of identical disc stacked together to form the trim. Each disc is divided into four sections (quarters) through which the fluid flows within the trim. Each quarter consists of a staggered arrangement of columns, in case of a multi-stage continuous-resistance trim. The plug slides along the bore of the trim to control the valve opening.

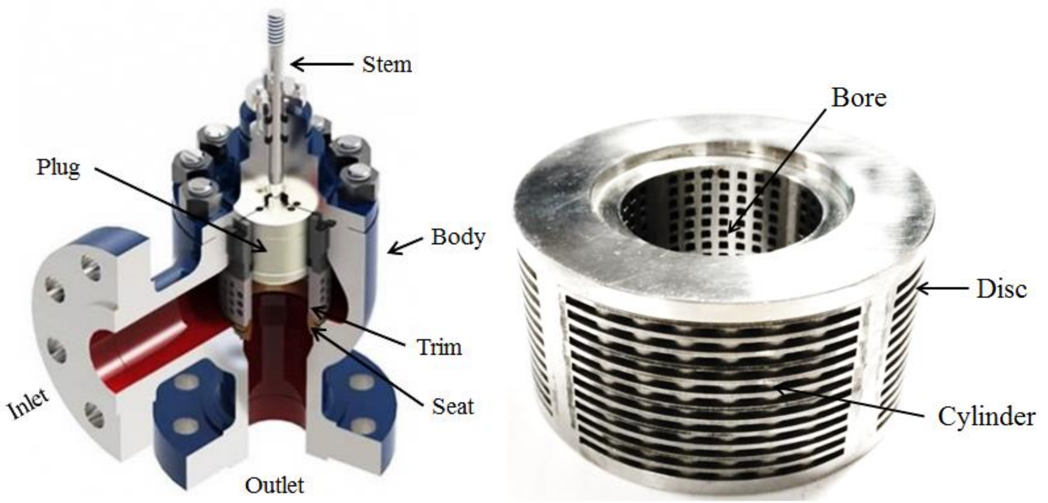

Figure 1 Different components of a control valve

The performance of a control valve or any of its components can be quantified in the form of its Flow Capacity (Cv) as [1-2]:

$$Q = Cv\,\beta\;\gamma\,\eta\sqrt{\frac{\Delta P}{\frac{\rho}{\rho_o}}} \qquad (1)$$

where ΔP and Q are the differential pressure and volumetric flow rate of fluid passing through the valve or the component. In equation (1), β is a numerical constant that depends on the units of Q and ΔP, γ is the factor that depends on the Reynolds number, η is piping geometry factor, ρ is the density of the fluid and ρ_o is the density of water. As equation (1) is applicable to both the control valve and its components, it can be easily measured for the control valve, the valve body and the seat through conventional experimental procedures. However, measuring the flow capacity of the trim through experimental methods locally is quite complex. Hence, an indirect method of finding the flow capacity of the trim has been reported in many different research studies conducted [3-4]. The flow capacity of the trim can therefore be computed as:

$$Cv_{\mathrm{Trim}} = \frac{1}{\sqrt{\left(\frac{1}{{Cv_{\mathrm{Valve}}}^2}\right)-\left(\frac{1}{{Cv_{\mathrm{Body}}}^2}\right)-\left(\frac{1}{{Cv_{\mathrm{Seat}}}^2}\right)}} \qquad (2)$$

As discussed earlier, a trim further comprises of discs, quarters, rows and flow paths, and quantifying the flow capacity of each of these sections of the trim is extremely difficult through experimental procedures. However, with the advent of power computing resources and Computational Fluid Dynamics (CFD) based techniques, it has become possible to evaluate the flow capacity of different sections of a trim numerically. Moreover, the numerical techniques allow investigating the complex flow behaviour within the different sections of a trim. Green et al [5-6] numerically investigated the flow behaviour within the different rows of a multi-stage continuous-resistance trim. Single phase CFD simulations have been carried out to analyse the velocity profiles within flow paths, and the pressure drop across the trim. It has been reported that local peak velocity causes significant increase in erosion within the trim. It has been stated that the numerical results need to be used with caution as it may be difficult to accurately simulate flow field both globally and locally.

Asim [7] has carried out extensive numerical investigations on the local flow behaviour within different multi-stage continuous-resistance trims. It has been reported that the pressure within these trims drops in a systematic manner, thus avoiding cavitation. It has also been shown that the flow capacity of these trims is independent of the process conditions. The effects of the manufacturing method used to produce these trims have been analysed. It has been shown that trims manufactured using Electric Discharge Machining (EDM) result in higher flow capacity compared to the trims manufactured using Selective Laser Melting (SLM) due to the different types of surface finishes achieved on the valves produced from these two manufacturing methods. Semi-empirical models have been developed to correlate the surface finish of a trim to its flow capacity. Charlton [8-9] extended this work to investigate the factors contributing to different surface finishes resulting from these two methods. It has been shown that joining the columns in alternative rows (to prevent flow mixing) results in significant flow reversals and recirculation within the trim. Moreover, it has been concluded that as the surface roughness of the flow paths increases, the flow capacity of the trim decreases. Tear-drop shaped flow paths have been shown to resist the onset of cavitation within multi-stage continuous-resistance trims.

Asim et al [10] carried out numerical investigations on the effects of valve opening position on the flow capacity of a multi-stage continuous-resistance trim. It has been reported that as the valve opening position increases, the flow capacity of the trim also increases. It has been concluded that the flow paths formed by circular cylinders depict linear opening characteristics. Lisowski and Filo [11] numerically investigated geometrical modifications to the stem of a proportional control valve for improved flow characteristics. Stems having circular and triangular holes have been analysed. It has been shown that triangular openings increase the proportional operating range of the valve by 40%. Hence, the shape and size of the openings through which the flow has to take place in a control valve, has a significant effect on the flow capacity. Zhou et al [12] developed a simplified methodology in order to quantify the flow capacity of a valve. Extensive CFD based investigations have been carried out to accurately quantify the fundamental flow parameters within a valve. Sun et al [13] numerically analysed the effects of surface finish on the flow capacity of a valve. It has been reported that surface finish significantly affects the flow capacity of a valve. As the manufacturing method has a considerable effect on the surface finish (as reported by Charlton [8-9]), the study lacks in quantifying the manufacturing parameters that affect the valve performance.

Asim et al [14] analysed the velocity profiles within the flow paths of a multi-stage continuous-resistance trim. It has been shown that the local flow behaviour within a trim is significantly influenced by the geometrical characteristics of the flow paths. Poorly designed flow paths can lead to higher erosion rates in the trim. A semi-empirical correlation has been developed to quantify the flow capacity of the trim by measuring the flow capacity of a flow path. Oliveira [15] has carried out experimental and numerical investigations on the flow capacity of multi-stage continuous-resistance trims, comprising of three different shapes i.e. circular, elliptical and tear-shaped columns. It has been shown that changing the geometrical features of the flow paths of a trim, significantly influences its flow capacity. Kong et al [16] analysed the flow field decomposition and its reconstruction for modelling the hydrodynamic characteristics of a valve. The transient flow fields have been reconstructed using Proper Orthogonal Decomposition (POD). Only a finite number of energy modes have been considered for this purpose. It has been shown that it is possible to accurately compute the flow rate and the force acting on the stem using reconstructed flow field within the valve.

Published literature suggests that although many recent studies have been carried out to analyse the local flow behaviour within multi-stage continuous-resistance trims, a systematic investigation into the effects of flow paths' geometrical features on the valve characteristics is yet to be quantified. Only qualitative analyses have been carried out in those studies where the effects of the geometrical features of flow paths have been investigated. In the present study, systematic numerical investigations have been carried out to quantify the effects of flow paths' geometrical features on the flow behaviour and flow capacity of the trim. For this purpose, novel flow related parameters have been developed to enumerate the pressure and energy loses within these trims. For effective comparison purposes, a conventional multi-stage continuous-resistance trim (having cylindrical columns) has been considered as the baseline. The conventional experimental testing methodology to quantify the flow capacity of the control valve is discussed in the following section, which will also be used for validation of numerical results.

2.0 Flow loop testing of a control valve fitted with the baseline trim

Based on the experimental procedures detailed in BS EN 60534-2-4:5 [17-18] for the flow capacity quantification of a control valve, a flow-loop has been constructed, as shown in figures 2(a, b and c). A 1x1x1m water tank is connected to a centrifugal pump, consisting of a grade 14 cast iron impeller. The centrifugal pump has a shaft power of 24.1kW at duty point, while the motor has a rated power of 37kW at the nominal speed of 2900rpm. The rated voltage and maximum current of the motor are 3~400V at 50Hz and 65A respectively. The pump delivers a head of 54.7m and flow rate of 26.2l/s at the duty point. The pump and the motor are connected to an inertia base made of four parts gravel, 2 parts sand and 1 part cement mixture, as shown in figure 2(d). The 250mm deep inertia base is fixed to the floor through four anti-vibration mounts, consisting of springs with a maximum deflection of 20mm at optimum load conditions, where each mount can support up to 198.9kg of point load.

The centrifugal pump is connected to the test valve containing the baseline trim, shown in figure 2(e). The body of the test valve has been manufactured in A351 CF8M cast. As 80% of the control valves are pneumatically controlled by the actuators, the test valve used in the present study is fitted with a diaphragm based pneumatic actuator. The actuator is controlled by 4.5bar gauge air supply, and is made of stainless steel. The baseline trim model is made of a material known as TuskXC2700T using a 3D printing technique, known as Stereolithography, as shown in figure 2(f). Across the test valve, a non-intrusive differential pressure transducer has been installed to measure the differential pressure. The differential pressure transducer is based on piezo-resistive stainless steel sensor, with a pressure range of 20mbar to 16bar, supply of 12V DC and output of 0 to 20mA. The differential pressure transducer used can measure up to 2.5bar differential pressure, with an accuracy of ±0.5%. The differential pressure transducer feeds the current data to an AC-DC converter, where a calibration equation is used to calculate the differential pressure across the control valve. The control valve is further connected to the gravitational water flow rate measuring system, also known as the hopper arrangement, as shown in figure 2(g). The hopper is attached to a load cell and a knife gate valve. The hopper arrangement can measure the mass flow rate of water based on load and time readings. The accuracy of the hopper arrangement is 0.1kg/s.

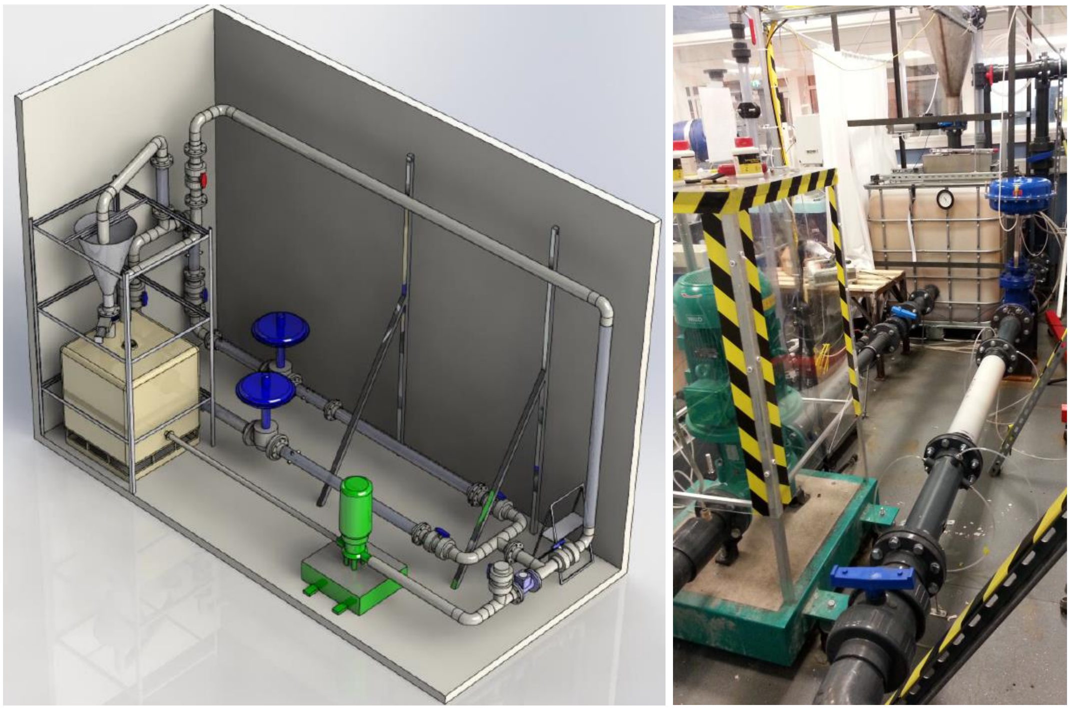

(a) (b)

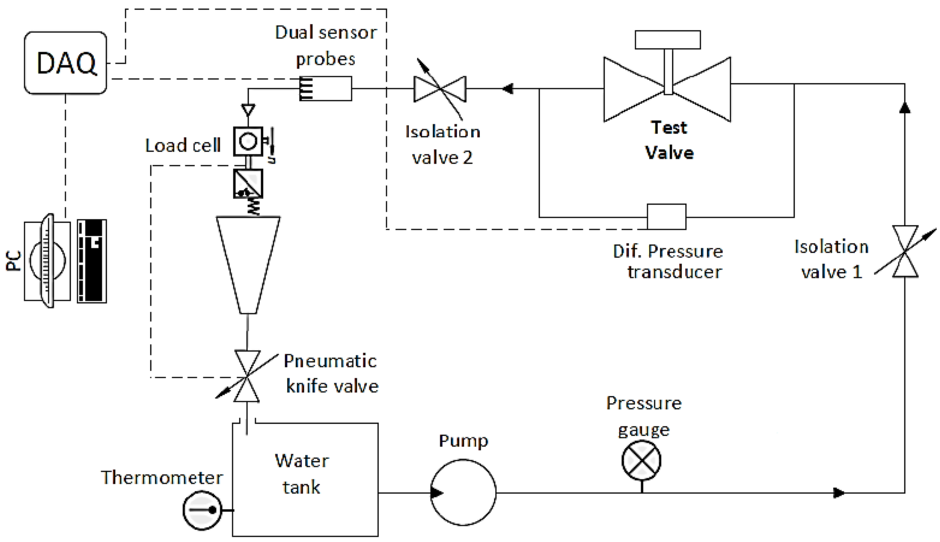

(c)

 

(d) (e)

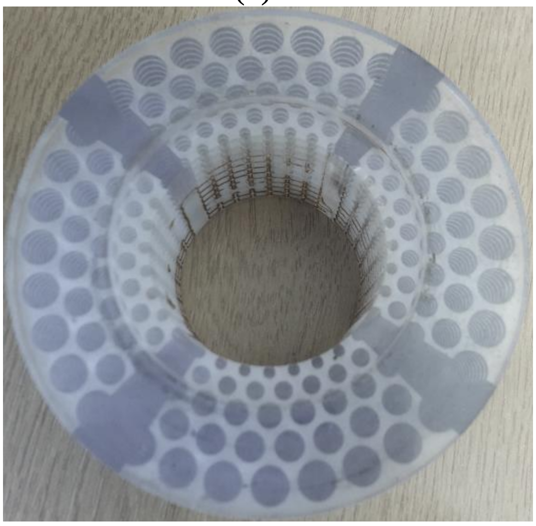 

(f) (g)

Figure 2 The flow-loop (a) 3D representation (b) facility (c) schematic representation (d) centrifugal pump (e) test valve (f) baseline trim model (g) hopper arrangement

According to BS EN 60534-2-3 [19], the test procedure for a control valve consists of a number of steps. These have been summarised in figure 3. The first step of the procedure is to record the atmospheric pressure and water temperature in order to compute the density of water (to be used in equation (1)). The next step is to set the valve opening position to 100%, and the pump set-point to maximum available flow. Flow loop is then run at these settings. The values of differential pressure (ΔP) and volumetric flow rate (Q) are recorded at-least three times. The average values of ΔP and Q are then used to compute the flow capacity of the valve (using equation (1)). Based on pre-known values of Cv_{Body} and Cv_{Seat}, the flow capacity of the trim is computed. The whole procedure, apart from the first step, is then performed at 80%, 60%, 40% and 20% VOPs. Similarly, tests are run at 50% and 25% of maximum available flow as recommended in BS EN 60534-2-3 [19].

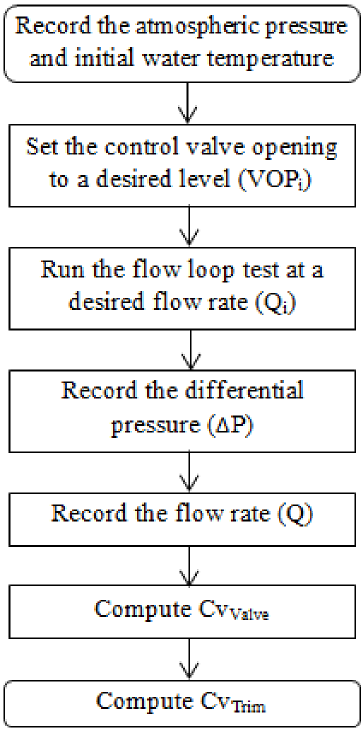

Figure 3 Flow chart of the test procedure

The flow capacity of the trim at various valve opening positions is shown in figure 4. It has been noticed that the flow capacity of the trim remains the same as the pump set-point varies, at a particular VOP. It is an established fact that the flow capacity of a trim is independent of the process conditions [5-10, 14-15], the same has been observed in the present study. Hence, only one curve, corresponding to maximum available flow rate, has been presented in figure 4. It can be seen that as the valve opening position increases, the flow capacity of the trim also increases. The flow capacity of the trim increases from 11.1 to 22.2 as the valve opening position increases from 20% to 40%. Further opening the valve to 60%, 80% and 100% increases the flow capacity of the trim to 32.6, 40.3 and 47.6 respectively. The increase in the trim's flow capacity has been observed to be linear, confirming that this particular trim is a linear opening trim.

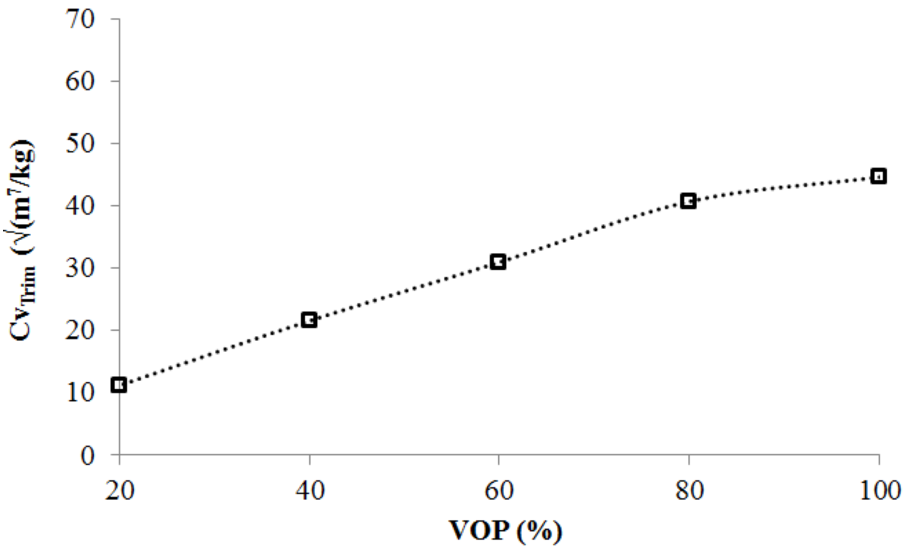

Figure 4 Variations in Cv_{Trim} at various valve opening positions

In order to analyse the effects of flow paths' geometrical features on the flow capacity of a multi-stage continuous-resistance trim, numerical investigations need to be carried out. A commercial Computational Fluid Dynamics (CFD) based solver has been used for this purpose. The detailed numerical modelling of the control valve is discussed in the following section.

3.0 Numerical modelling of the control valve

The globe type control valve considered in the present study, installed with the baseline multi-stage continuous-resistance trim (cylinders based), has been numerically modelled and analysed to quantify the flow capacity of the trim. Once the numerically predicted results are verified against the experimental results, detailed analyses of the complex flow behaviour within the trim will be carried out.

3.1 Geometry of the control valve and the baseline trim

The geometry of the control valve and the baseline trim is shown in figure 5. For effective comparison between the numerical and experimental results, the geometry has been modelled as realistically as possible. It has been shown in many research studies that the primary reason behind the differences between the numerical and experimental results is non-matching geometry [20-23]. Hence, based on control valve testing standards BS EN 60534-2-4:5 [17-18], inlet and outlet pipe section of lengths 2D and 6D have been attached at either ends of the control valve, where D is the diameter of the valve, as shown in figure 5(a). The flow direction in the trim is from outside, towards the centre of the trim, hence the trim/s considered in the present study has flow-over characteristics. Some important dimensional parameters of the trim have been defined here, as they will be used later in this study for analysis purposes. These include the radii of the entry and exit of the rows. It can be seen in figure 5(b) that the radius at the entry of the outermost row (or row 1) has been referred to as R_1, which is the same as the outer radius of the trim (R_{Out}). Similarly, the radius at the exit of row 1 is R_2, which is also the radius at the entry of row 2. The radius at the exit of the innermost row (row 5) is R_6. It must be noted that $R_1>R_2>R_3>R_4>R_5>R_6$.
The geometry of a single flow path is shown in figure 5(c). It can be seen that a flow path within a multi-stage continuous-resistance trim has geometrical features similar to a converging-diverging duct. The major and minor radii of curvature of either walls of the flow path have been shown as $r_{max,i}$ (OA) and $r_{min,i}$ (OB) for i^{th} row respectively, while the minimum distance between the walls (at the centre of the flow path) is shown as d_i for the same row of the trim. Hence, $r_{max,i}$, $r_{min,i}$ and d_i for row 1 will be represented as $r_{max,1}$, $r_{min,1}$ and d_1, while for row 5 these will be represented as $r_{max,5}$, $r_{min,5}$ and d_5. In case of a conventional multi-stage continuous-resistance trim (baseline trim), since the columns are cylindrical, $r_{max,i}=r_{min,i}$. It is noteworthy that multi-stage continuous-resistance trims regulate the fluid flow on the principle of area expansion in the direction of flow. Thus, the minimum distance between the walls of flow paths will keep on increasing in the flow direction i.e. $d_1<d_2<d_3<d_4<d_5$. In the present study, $r_{max,i}$ has been kept the same as in the baseline trim while the effects of $r_{min,i}$ variations on the flow capacity of the trim have been analysed.

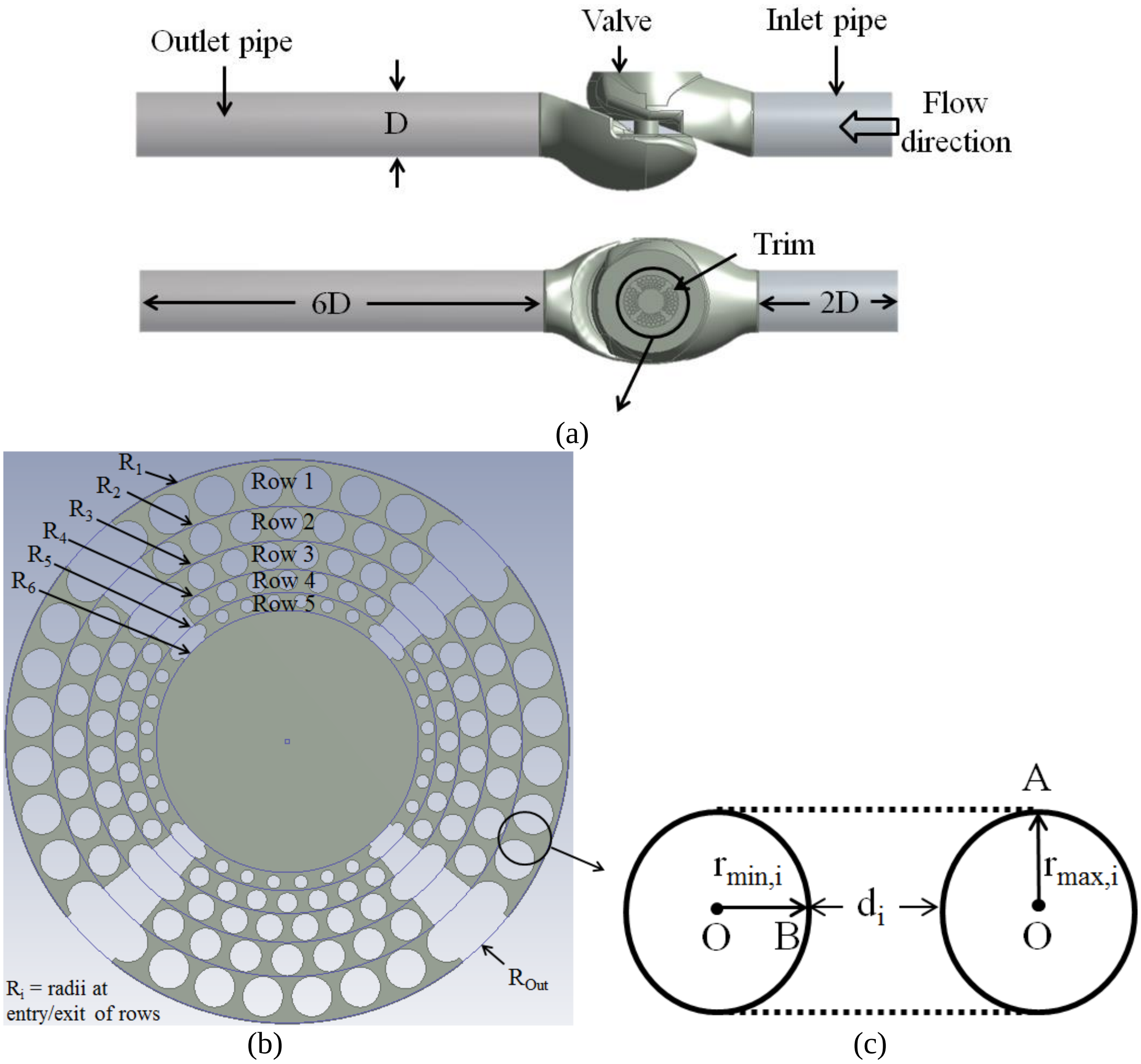

Figure 5 Geometric model of the control valve (a) flow domain (b) baseline trim (c) a flow path

3.2 Spatial Discretisation of the Control Valve

The control valve, containing the baseline trim, has been spatially discretised using different techniques for different valve sections. This has been purposefully carried out in order to accurately predict the complex flow features within the control valve in general, and the trim in particular. Hence, the inlet and outlet pipes have been spatially discretised using hexahedral elements, while the control valve (including the trim) has been spatially discretised using tetrahedral elements. Hexahedral elements are preferred in relatively simple geometries, and in the regions where the flow is uni-directional, due to less numerical diffusion associated with them [24-26]. Tetrahedral elements offer higher numerical diffusion compared to hexahedral elements, however, they are preferred in complex geometries and in the regions where the flow is highly non-uniform. Spatial discretisation of the control valve and the trim is shown in figure 6. In order to resolve the near-wall boundary layers within the flow paths of the trim, layers of hexahedral elements have been generated in close proximity of flow path walls, as shown in figure 5(b). A growth rate of 20% has been used within these layers, indicating that the thickness of consecutive layers is 20% more compared to the previous layer. It has been shown by Asim et al [14] that a 20% growth rate in the near-wall hexahedral mesh layers is capable of accurately predicting the boundary layer around the columns.

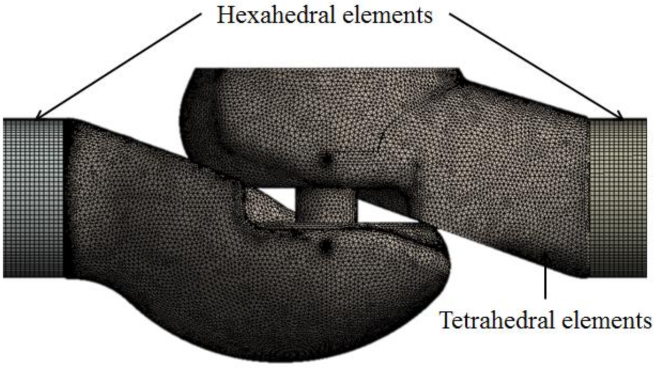

(a)

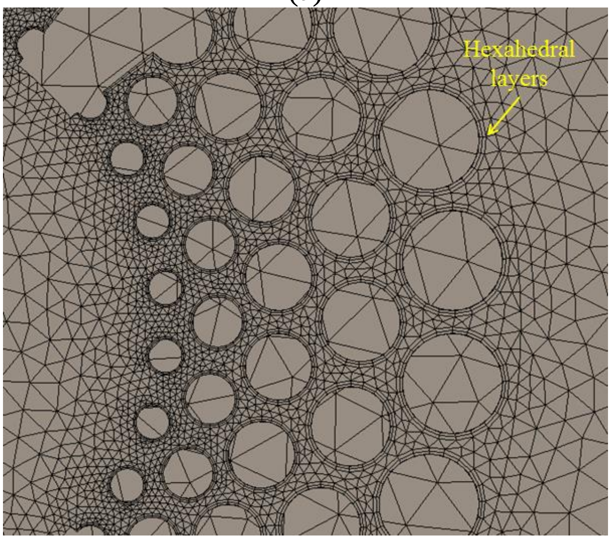

(b)

Figure 6 Spatial discretisation of the (a) control valve (b) baseline trim

3.3 Solver Settings

Specification of appropriate boundary conditions is critical to the accuracy of any numerical analysis [27-28]. In the present study, the inlet boundary of the flow domain has been specified as mass flow inlet, while the outlet boundary has been specified as pressure outlet. The mass flow rate specified at the inlet boundary has been kept the same as measured experimentally at individual valve opening positions. Thus, mass flow rates of 13.19kg/s, 12.06kg/s, 10kg/s, 6.98kg/s and 3.44kg/s have been specified at valve opening positions of 100%, 80%, 60%, 40% and 20% respectively. The outlet boundary of the flow domain has been specified with atmospheric pressure i.e. 101325Pa absolute. The walls in the flow domain (such valve body, flow path walls etc.) have been modelled as no-slip boundaries, as expected in real-world. Based on the initial water temperature (20^{o}C) and atmospheric pressure measured experimentally, a density of 998.2kg/m^3 has been specified to the working fluid i.e. water, having a dynamic viscosity of 0.001003kg/(m s). In order to resolve turbulence parameters numerically, Shear Stress Transport (SST) k-ω turbulence model has been used in the present study [29]. It has been shown in various research studies that SST k-ω turbulence model is better suited for control valve applications because of its superiority in predicting the complex flow features (like adverse pressure gradients) within valves [30-33].

This turbulence model comprises of a cross-diffusion term in turbulent dissipation rate equation, along-with a blending function, to ensure that the model behaves appropriately in both near-wall and far-field zones.

Reynolds Averaged Navier-Stokes (RANS) equations [34-35], along-with the mass conservation and turbulence parameters' equations, have been iteratively solved for steady flow of water within the control valve. A convergence criterion of 0.001 for continuity, momentum conservation and turbulence parameters has been specified. Moreover, solver convergence has been additionally judged on the basis of static pressure at the inlet boundary of the flow domain. Figure 7 depicts the static pressure variations at the inlet boundary (P_{in}). It can be seen that there are significant variations present in the first 50-100 iterations of the solver. After that, the solver stabilises considerably, giving rise to consistent pressure values.

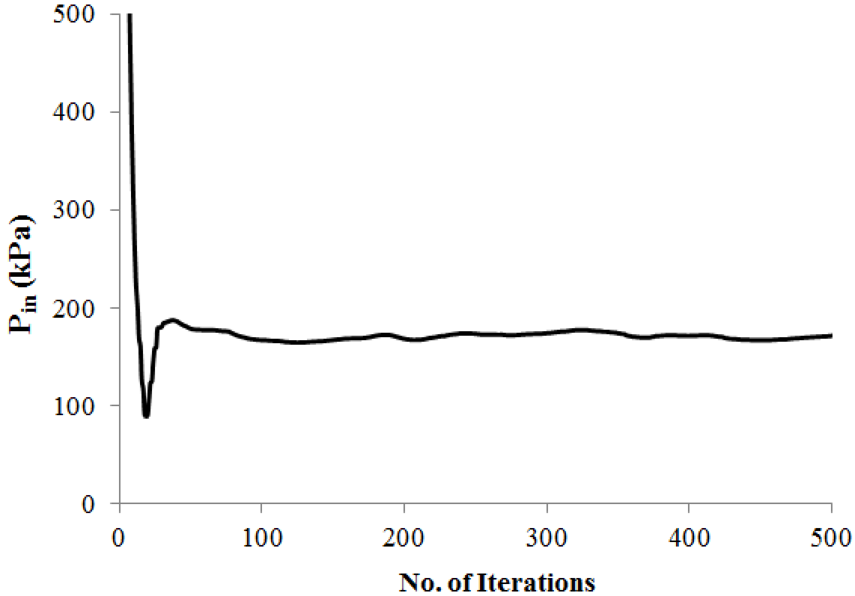

Figure 7 Solver convergence

3.4 Mesh Independence Testing

Although the reliability of the numerically predicted results is dependent on solver convergence, the accuracy of the results is dependent on mesh independence. Mesh independence is the process through which it is assured that the numerical results are independent of the various factors that affect the spatial discretisation of the flow domain [36]. A mesh independence study has been carried out using four different mesh configurations i.e. 3.4 million, 4.3 million, 5.3 million and 6.5 million mesh elements. The variations in the static pressure at the inlet boundary of the flow domain have been shown in figure 8. It can be seen that the inlet static pressure, predicted by mesh having 3.4 million elements, is the lowest of all mesh configurations considered. The other three mesh configurations depict relatively similar inlet pressure values.

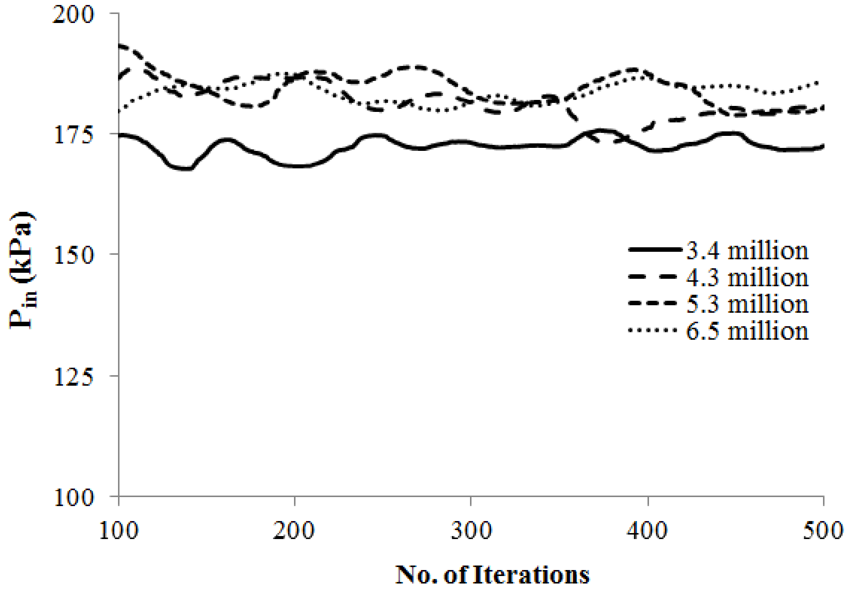

Figure 8 Variations in inlet static pressure for different mesh configurations

To further analyse the effect of the number of mesh elements on P_{in}, average values of P_{in} (for the last 100 iterations) have been computed and summarised in table 1. It can be noticed that by increasing the number of mesh elements from 3.4 million to 4.3 million elements, the average static pressure at the inlet boundary of the flow domain increases by 5.1%. Further increasing the number of elements to 5.3 million increases the inlet pressure by 1.9%. Finally, increasing the number of elements from 5.3 million to 6.5 million, the average static pressure decreases by 0.9%. As the difference in the average inlet pressure values between 5.3 million and 6.5 million elements is less than 1%, the mesh with 5.3 million elements has been chosen in the present study for further analysis.

Table 1 Average inlet static pressure comparison

No. of Mesh Elements (million)	Average P_{in} (kPa)	Difference in average P_{in} (%)
3.4	172.8	-
4.3	181.6	5.1
5.3	184.9	1.9
6.5	183.3	-0.9

3.5 Benchmark Testing

Validation of the numerically predicted Cv_{Trim} has been carried out by comparing it with the experimentally found Cv_{Trim} values at various valve opening positions. It can be clearly seen in figure 9 that the numerically predicted flow capacity of the baseline trim model, at all valve opening positions, matches closely with the experimentally measured Cv_{Trim} values. The figure also depicts the percentage differences between the two results at individual valve opening positions. It can be noticed that the minimum difference between the two results is 0.6% at 20% VOP, and the maximum difference is 6.7% at 100% VOP. The average difference between numerically predicted and experimentally measured Cv_{Trim} is 2.6%, which is acceptable. It should however be noted that these differences arise due to a number of factors affecting the experimental and numerical results, such as the surface roughness of the trim and the valve, accuracy of the measuring instruments, accuracy of the turbulence modelling etc.

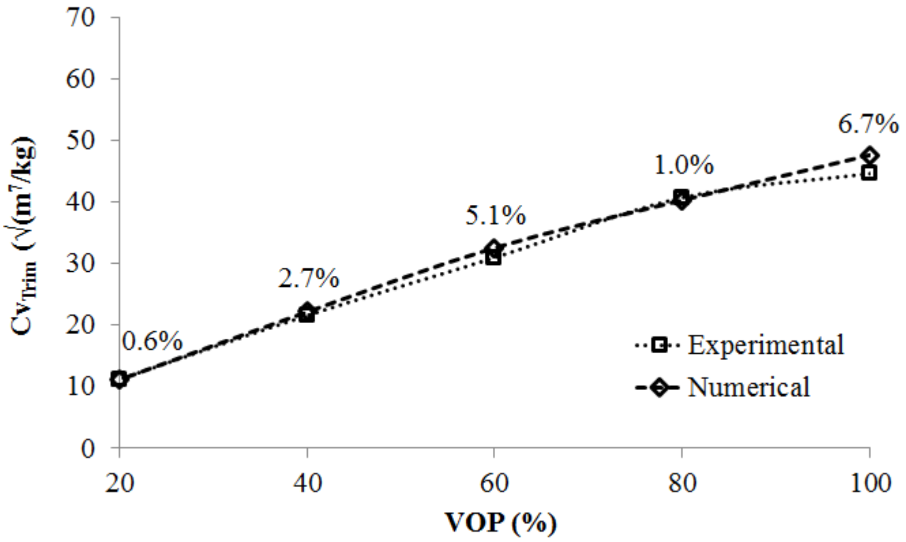

Figure 9 Comparison of numerical and experimental Cv_{Trim} of the baseline trim

4.0 Flow behaviour within the baseline trim

The flow field within multi-stage continuous-resistance trims have been depicted in the form of pressure and velocity fields. The pressure field has been quantified in terms of a non-dimensional parameter defined as $\frac{P_{in}-p}{P_{in}}$ where P_{in} is the static pressure at the inlet of the flow domain, while p is the local static pressure within the trim. This parameter represents relative pressure drop within the trim with inlet pressure being the reference pressure. Hence, higher values of non-dimensional pressure parameter will indicate relatively higher change in static pressure with respect to the inlet pressure, and hence higher pressure drop. Detailed analysis of non-dimensional pressure field within multi-stage continuous-resistance trims will help in understanding the complex flow behaviour within such trims.

Variations in non-dimensional pressure parameter within the top disc of the baseline trim at 100% VOP are depicted in figure 10. The top disc of the trim has been chosen for analysis because it has been reported in earlier studies [5-10] that all the discs of a multi-stage continuous-resistance trim behave in the same manner hydrodynamically. It can be seen in figure 10 that at the entry of the trim (outermost row), the non-dimensional pressure is almost zero. This indicates that pressure at the entry of the trim is the same as at the inlet of the flow domain (i.e. line-pressure), as expected. As the flow enters the flow paths of row 1, the non-dimensional pressure increases, indicating that static pressure here is substantially lower than line-pressure. However, on exit from flow paths of row 1, the non-dimensional pressure decreases. This trend is followed throughout the trim up-till the exit of row 5, where the non-dimensional pressure is high (and hence static pressure is low compared to line-pressure). As there are no more rows available after row 5, the flow from all the quarters of the trim accumulates in the bore region, and then propagates to the outlet of the valve. Hence, it is clear from the figure that static pressure drops within a multi-stage continuous-resistance trim in a series of steps, which helps in regulating the flow. The reason for higher non-dimensional pressure in the flow paths of each row is the fact that flow paths offer area reduction; significantly decreasing the static pressure at the centre of flow paths. Quantitatively, the average non-dimensional pressure at the entry and exit of row 1 has been computed to be 0.008 and 0.103, which means that the pressure at the entry and exit of row 1 is 0.8% and 10.3% lower than at the inlet of the flow domain respectively. Hence, the non-dimensional pressure drop across row 1 of the baseline trim is 9.5% of the inlet pressure. Similarly, non-dimensional pressure drop across rows 2, 3, 4 and 5 has been computed to be 5.8%, 8.7%, 5.4% and 5.3% of the inlet pressure respectively. It can be seen that non-dimensional pressure drop decreases by 39.3% from row 1 to row 2, while in increases by 50.5% from row 2 to row 3. It again decreases by 38% from row 3 to row 4, while slightly decreasing (by 1.4%) from row 4 to row 5 of the baseline trim. It can be noticed that the non-dimensional pressure drop across the inner rows of the trim (i.e. rows 4 and 5) is around 5.3% of line-pressure and remains almost constant. This is because the central gap between the walls of flow paths (d_i) increases considerably, resulting in relative reduction in resistance to the flow. Because the flow channel geometry is considerably affected by the choice of $r_{max,i}$ and $r_{min,i}$, which in-turn dictates the resistance to the flow, therefore it can be concluded that the geometrical features of a flow path significantly influences the flow behaviour within multi-stage continuous-resistance trims.

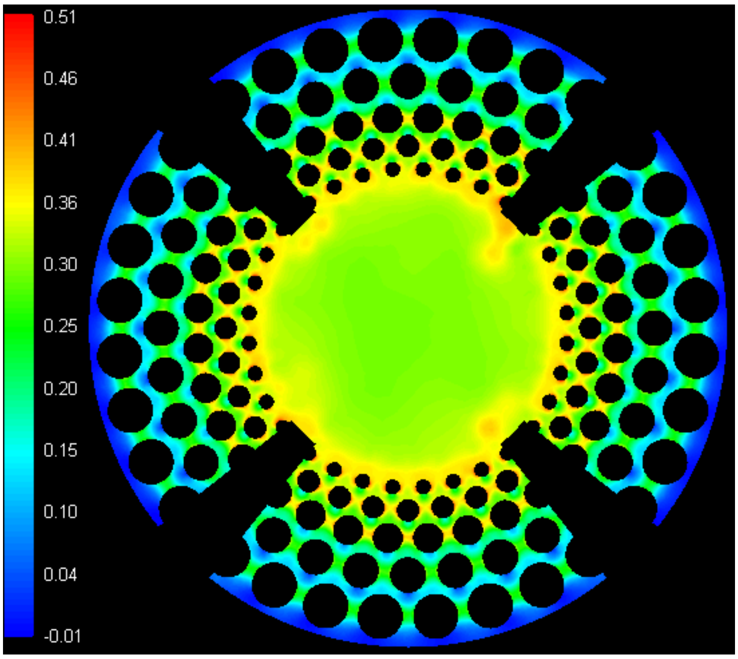

Figure 10 Variations of non-dimensional pressure within the baseline trim

In order to quantify flow velocity variations within the baseline trim, a non-dimensional flow velocity distribution parameter has been used here. The flow velocity (magnitude along-with the three cylindrical components) has been non-dimensionalised with average flow velocity magnitude at the inlet of the flow domain (V_{in}). Hence, the flow velocity distributions shown here are of the form v/V_{in}. Figure 12 depicts the non-dimensional flow velocity magnitude variations ($|v|/V_{in}$) within the top disc of the trim at 100% VOP, where v is the local flow velocity magnitude. It can be seen that the non-dimensional flow velocity magnitude is highest in the flow paths in each row, while it is lower at the entry and exit of the rows. The highest non-dimensional flow velocity magnitude has been recorded in flow paths of row 3, corresponding to the maximum pressure drop trends discussed earlier. It can be further seen that the velocity profiles in flow paths of rows 1 to 3 are symmetric i.e. the flow velocity is highest in the centre of flow paths and decreases proportionally towards the walls on either sides of flow paths, as observed by Asim et al [14]. However, in case of rows 4 and 5, the velocity profiles are non-symmetric in flow paths. The reason for this non-symmetric behaviour of flow velocity in flow paths of rows 4 and 5 is the geometrical characteristics of these flow paths; the central gap between the walls of flow paths (d_i) is quite large. The average non-dimensional flow velocity magnitude at the entry and exit of row 1 has been computed to be 1.17 and 2.29 respectively. This means that average flow velocity magnitude at the entry and exit of row 1 is 17% and 129% higher than V_{in} respectively. Similarly, non-dimensional flow velocity magnitude at the exit of rows 2, 3, 4 and 5 has been recorded to be 2.46, 2.81, 2.57 and 2.57 respectively. It can be noticed that the highest average flow velocity magnitude is recorded at the exit of row 3, while the flow velocity remains constant at both the entry and exit of row 5.

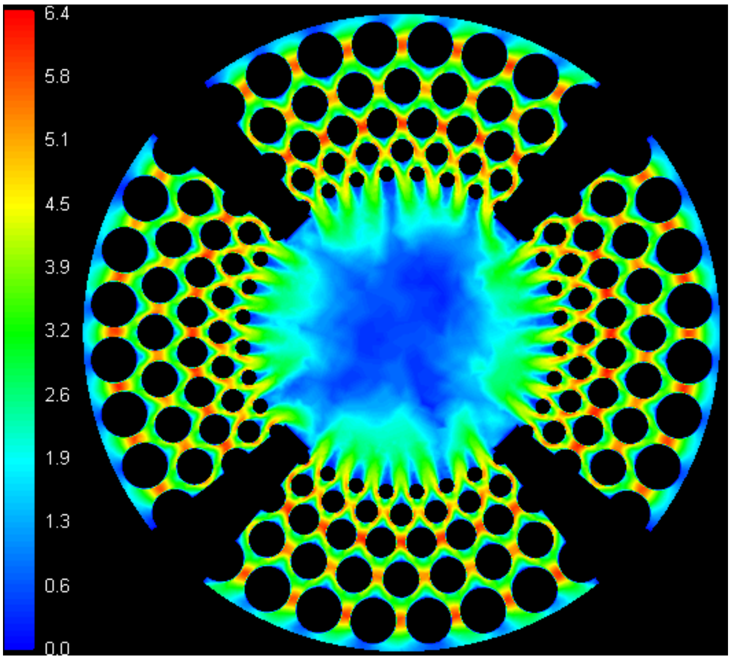

Figure 11 Variations of non-dimensional flow velocity magnitude within the baseline trim

For further analysis of the flow velocity distribution within the baseline trim, normalised radial (v_r/V_{in}), tangential (v_θ/V_{in}) and axial (v_z/V_{in}) components of the flow velocity within a single quarter of the top disc (right quarter in figure 11, which is aligned with the incoming flow) have been depicted in figure 12. The scale of these variations clearly shows that the primary flow velocity component in a multi-stage continuous-resistance trim is the radial component, followed by the tangential component (in magnitude). The axial flow velocity component (figure 12(c)) is negligible. It can be seen in figure 12(a) that normalised radial velocity variations are similar to velocity magnitude variations shown in figure 11. However, the normalised tangential velocity (in figure 12(b)) is higher at the entry and exit of flow paths, while it is lowest in the flow paths where flow areas are smaller. This is because when the flow exits a flow path, it is diverted by the walls of the next row's flow paths. Hence, the tangential velocity increases. Similarly, upon entering a flow path, flows exiting from either side of the previous row's flow paths, combine and enter the flow path. Therefore, the tangential flow velocity component is higher at the entry and exit of flow paths. A summary of normalised average radial and tangential velocity components, at the entry/exit of each row of the baseline trim, has been presented in table 2.

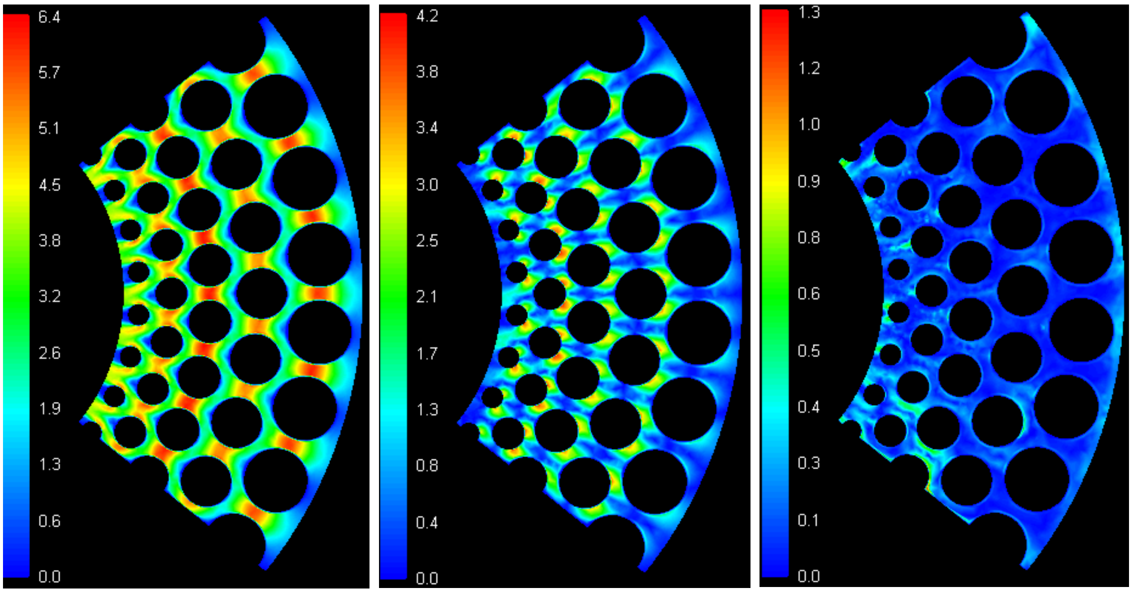

(a) (b) (c)

Figure 12 Variations in flow velocity components of the baseline trim model (a) radial (b) tangential (c) axial

It can be seen that the normalised average radial velocity is higher than the normalised tangential velocity, on average across the trim. However, the normalised average tangential velocity at the entry of rows 2, 3 and 4 is higher than the normalised average radial velocity. Hence, average tangential velocity in the central rows of the baseline trim is higher than the average radial velocity. This can also be attributed to the geometric features of the flow paths in rows 2 and 3, where the central gap between the walls of flow paths is considerably less than in rows 4 and 5.

Table 2 Variations in normalised average flow velocity components at the entry/exit of different rows of the baseline trim

	v_r/V_{in}	v_θ/V_{in}
Row 1 entry	1.01	0.36
Row 2 entry	1.30	1.76
Row 3 entry	1.51	1.85
Row 4 entry	1.77	2.07
Row 5 entry	2.02	1.44
Row 5 exit	2.44	0.51

It has been seen from the pressure and velocity fields that the flow field is highly three-dimensional near the cylinders of the trim. Highly three-dimensional flows are associated with higher energy losses, and hence, an energy loss analysis has been carried out in the present study to quantify energy efficiency of the trim. The total energy loss through the trim will depend on the local flow characteristics and energy losses taking place along the flow path, and hence, a local energy loss analysis has been carried out using local pressure and velocity values. The variation in energy loss parameter (ζ) is representative of the change of energy across the different rows of the trim. Hence, the energy loss parameter ζ can be expressed as:

$$\zeta = \frac{(p_i - p_{i+1})}{\rho g} + \frac{V_i^2 - V_{i+1}^2}{2g} \quad (3)$$

where p_i and V_i are the average static pressure and flow velocity magnitude upstream the i^{th} row of the trim, ρ is the density of water and g is the gravitational acceleration. The terms p_i-p_{i+1} and V_i-V_{i+1} refer to the change in average static pressure and flow velocity magnitude across a row of the trim. Thus, the first term on the RHS of equation (3) represents static head loss, while the second term represents dynamic head loss (in meters).

Variations in energy loss parameter (ζ) across the different rows of top disc of the baseline trim, at 100% VOP, have been shown in figure 13. The X-axis of the figure represents the radial direction; R_i/R_{out}=1 indicates the entrance of the trim (entry of row 1), while a value of 0.53 refers to the exit of row 5. It can be seen that as the flow propagates along the trim, it loses its energy. The energy loss across row 1 of the trim is 1.45m (of water). The energy loss across row 2 of the trim is 1.1m. Hence, the energy loss in row 2 of the trim is 23.9% less than in row 1 of the trim. Similarly, the energy loss across rows 3, 4 and 5 of the baseline trim is 1.57m, 1.32m and 1.12m respectively. It can be noticed that the energy loss across row 3 of the trim is highest, while across row 5 is the lowest

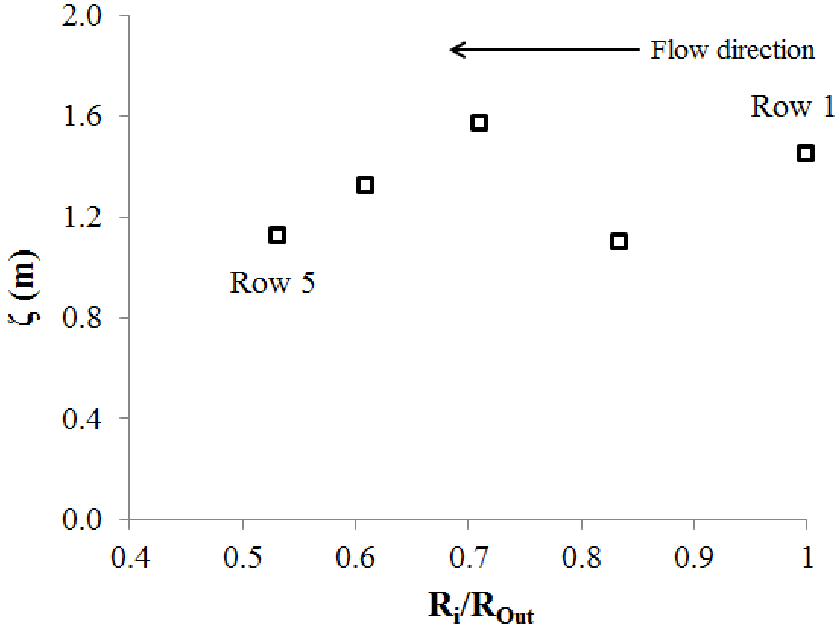

Figure 13 Variations of energy loss parameter within the baseline trim

In order to explain this non-uniform behaviour of energy loss in the baseline trim, a central gap ratio parameter (d_{i+1}/d_i) for the flow paths in each row has been calculated. In this parameter, d_{i+1} is the central gap between the walls of a flow path of a particular row, while d_i is the central gap between the walls of a flow path from previous row. Hence, if $1<d_{i+1}/d_i$, flow path is offering area expansion to the flow, while if $d_{i+1}/d_i<1$, flow path is offering area contraction to the flow. Moreover, less energy loss is expected if area expansion is offered, while more energy loss is expected if area contraction is offered. It has been established through the present design that d_{i+1}/d_i for row 1 is equal to 1 (as expected, as there is no row before row 1). Similarly, d_{i+1}/d_i for rows 2 to 5 is 1.13, 0.89, 1.21 and 1.26 respectively. It can be noticed that row 2 is offering area expansion, and thus, energy loss across the flow paths of row 2 is less than across row 1. However, row 3 is offering area contraction (and thus higher energy loss). Flow paths of rows 4 and 5 offer area expansion, associated with reduction in energy loss.

From the above discussions, it is clear that the geometric features of flow paths of a multi-stage continuous-resistance trim affect the flow behaviour and performance of the trim considerably. Hence, it may be possible to regulate the flow field within the trim through careful manipulation of $r_{min,i}$ (and hence d_i) and achieve desirable flow field characteristics.

5.0 Effects of the central distance between flow paths' walls (d_i) on the flow capacity of the trim

Four configurations of the multi-stage continuous-resistance trim have been used to investigate the effects of the central gap between the walls of flow paths (d_i), on the flow capacity of the trim. As shown in figure 5(c), d_i is dependent on the radii of flow path walls i.e. $r_{max,i}$ and $r_{min,i}$. In the present study, $r_{max,i}$ has been kept constant (same as the baseline trim), while $r_{min,i}$ has been decreased in order to increase the central gap between the walls of flow paths. The major radii ($r_{max,i}$) have been kept constant for effective comparison against the baseline trim (decreasing the major radii will decrease the overall size of the columns, offering less resistance and hence, higher flow capacity). The minor radii ($r_{min,i}$) have been decreased because it has been analysed in the previous section that the baseline trim is offering substantial resistance to the flow (and hence higher energy loss). The minor radii configurations considered in the present study for further analyses are $0.9r_{min,i}$, $0.8r_{min,i}$, $0.7r_{min,i}$ and $0.6r_{min,i}$. Hence, major-to-minor radius ratio considered are $r_{max,i}/r_{min,i}$ = 0.9, 0.8, 0.7 and 0.6. The resulting central gaps between the walls of flow paths of the modified trim configurations, per the central gaps in the baseline trim, have been summarised in table 3. It can be clearly seen that as $r_{max,i}/r_{min,i}$ decreases, the central gap between the walls of flow paths increases.

Table 3 Ratio of the central gaps between the walls of flow paths of modified trims and the baseline trim

	$\frac{d_{i,0.9}}{d_{i,baseline}}$	$\frac{d_{i,0.8}}{d_{i,baseline}}$	$\frac{d_{i,0.7}}{d_{i,baseline}}$	$\frac{d_{i,0.6}}{d_{i,baseline}}$
Row 1	1.46	1.91	2.37	2.82
Row 2	1.49	1.85	2.21	2.57
Row 3	1.31	1.61	1.92	2.22
Row 4	1.45	1.67	1.90	2.13
Row 5	1.69	1.84	2.00	2.15

Numerical simulations at various valve opening positions have been run, and the flow capacity of the modified trims has been enumerated, as shown in figure 14. It can be seen that as the central gap between the walls of flow paths increases, the flow capacity of the trim also increases (as expected due to less resistance to the flow). However, this trend is observed in the range of VOP from 20% to 80% only. At 100% VOP, this trend changes for the trims having $r_{max,i}/r_{min,i}$ = 0.7 and 0.6; Cv_{Trim} for both $0.7r_{min,i}$ and $0.6r_{min,i}$ trims is less than $0.8r_{min,i}$ trim. Moreover, it has also been noticed that for $0.7r_{min,i}$ trim, Cv_{Trim} at 100% VOP is the same as at 80% VOP, while for $0.7r_{min,i}$ trim, Cv_{Trim} at 100% VOP is less than at 80% VOP.

This clearly suggests that although $0.9r_{min,i}$ and $0.8r_{min,i}$ trims are linear opening trims (like the baseline trim), $0.7r_{min,i}$ and $0.6r_{min,i}$ trims are acting like quick opening trims. Hence, it can be concluded from these results that as the central gap between the walls of flow paths increases, the flow capacity of the trim increases up-till a certain central gap value, after which, further increase in the central gap between the walls of flow paths changes the inherent opening characteristic of the trim.

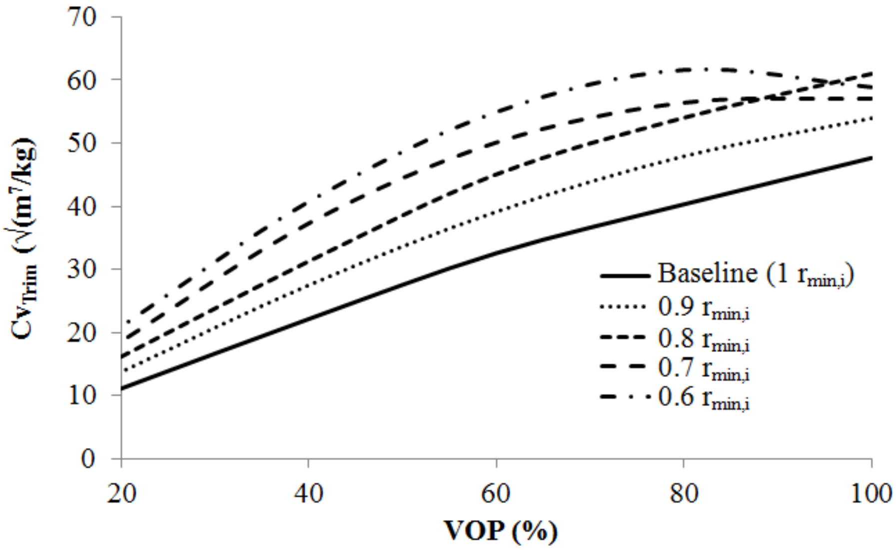

Figure 14 Comparison of Cv_{Trim} between the baseline and modified trim configurations

It is important at this stage to analyse the flow behaviour within a quick opening trim ($0.6r_{min,i}$ here) to understand the reasons for the change in the inherent opening characteristics of the trim. Hence, figure 18 depicts the variations of non-dimensional pressure within the top disc of the trim at 100% VOP. In comparison with figure 10, it is evident from the scale of the variations that the pressure drop within $0.6r_{min,i}$ trim is significantly lower than in the baseline trim, although the general qualitative trend in non-dimensional pressure distribution remains the same. The reason for less pressure reduction in $0.6r_{min,i}$ trim is the fact that there is more central gap between the walls of flow paths, hence, there is less resistance to the flow. The non-dimensional pressure drop across rows 1 to 5 of $0.6r_{min,i}$ trim is 1.0%, 0.7%, 1.0%, 0.8% and 0.8% of the inlet pressure respectively. In comparison with the baseline trim, the non-dimensional pressure drops across rows 1 to 5 of $0.6r_{min,i}$ trim is 98.7%, 87.7%, 89.0%, 85.4% and 85.4% lower. Hence, on average, the pressure drop across $0.6r_{min,i}$ trim is 87.4% less than the baseline trim, however, further analysis is required to establish the reasons for the change in the inherent opening characteristics of the trim.

Further analysing the flow behaviour within a quick opening trim, in comparison with a linear opening trim (i.e. baseline trim), it can be seen in figure 16 that the variations in non-dimensional flow velocity magnitude are substantially different from the one observed in figure 11 in the baseline trim. The non-dimensional flow velocity magnitude remains almost the same in flow paths of row 1, while it increases slightly in row 2. There is considerable increase in non-dimensional flow velocity in flow paths of row 3, however, higher flow velocity regions can be seen to be restricted to an area in close-proximity of the columns, rather than covering the entire flow path (as seen in the baseline trim). Non-dimensional flow velocity magnitude distribution within rows 4 and 5 matches more closely with the baseline trim. On average, it is evident from the scale of variations that non-dimensional flow velocity magnitude in $0.6r_{min,i}$ trim is considerably lower than in the baseline trim. Moreover, it has

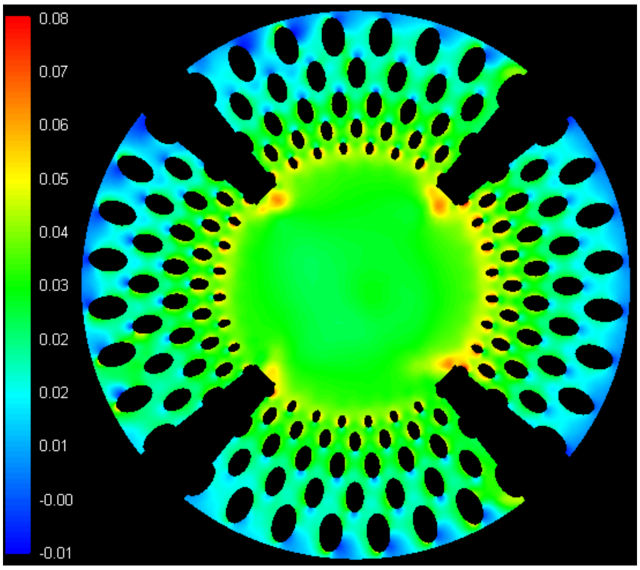

Figure 15 Comparison of differential pressure within the baseline and $0.6r_{min,i}$ trims

been computed that average non-dimensional flow velocity magnitude at the exits of rows 1 to 5 is 60.9%, 58.9%, 58.8%, 52.3% and 47.5% lower than the baseline trim. Hence, an important observation in a quick opening trim, as opposed to a linear opening trim, is that the flow velocity magnitude in the flow paths of outer rows remains almost constant, and the same as at the entry and exit of these rows.

For further analysis of the flow velocity distribution within the quick opening trim, figure 17 has been used which depicts the variations in normalised radial and tangential velocity components. Apart from the scale of these variations, which is considerably lower in $0.6r_{min,i}$ trim as compared to the baseline trim, the normalised radial velocity distribution matches closely with the flow velocity magnitude distribution, and hence, quite different to the baseline trim. However, the normalised tangential velocity distribution in both the baseline and $0.6r_{min,i}$ trims are qualitatively similar. A quantitative comparison of the normalised radial and tangential velocity components, between the baseline and $0.6r_{min,i}$ trims, is presented in table 4.

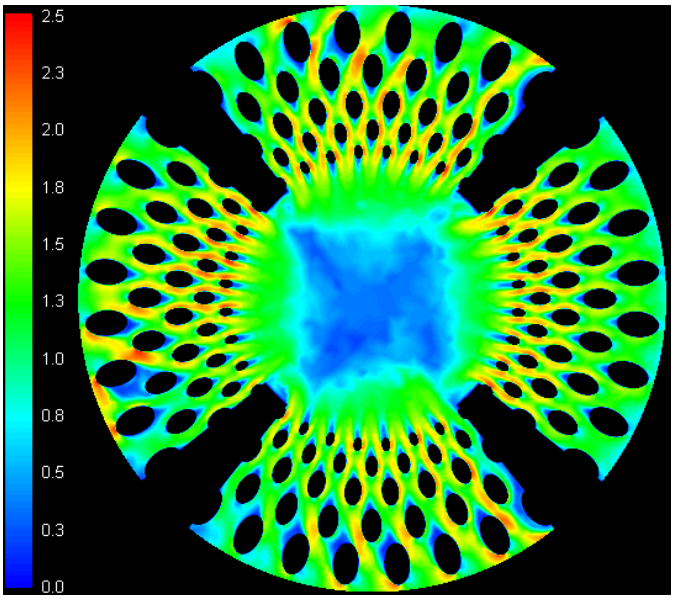

Figure 16 Comparison of flow velocity magnitude within the baseline and $0.6r_{min,i}$ trims

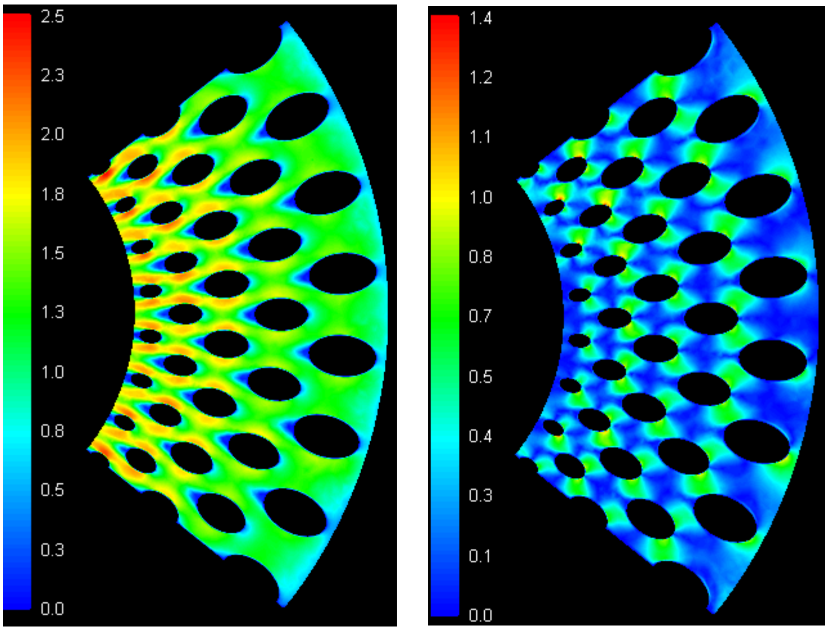

(a) (b)

Figure 17 Comparison of flow velocity components within the baseline and $0.6r_{min,i}$ trims (a) radial (b) tangential

The analyses of flow behaviour within the quick opening trim ($0.6r_{min,i}$) has provided some indications as to why a trim's inherent opening characteristic changes. However, a detailed quantitative analysis is still required. Hence, the variations in the energy loss parameter (ζ) for the different trims considered up-till now is shown in figure 18. It can be clearly seen that as the central gap between the walls of flow paths increases, the energy loss across the trim decreases. For all the linear opening trims (baseline, $0.9r_{min,i}$ and $0.8r_{min,i}$), there are significant variations in energy loss across the different rows of the trim. However, in case of quick opening trims ($0.7r_{min,i}$ and $0.6r_{min,i}$), the variations in energy loss across the different rows of the trim are almost constant, especially in case of $0.6r_{min,i}$ trim. Hence, it can be concluded that the energy loss across the different rows of a quick opening trim remains constant, while it varies considerably for linear opening trims.

Table 4 Comparison of normalised radial and tangential velocity components between $0.6r_{min,i}$ and the baseline trims

	$\dfrac{\left(\frac{V_r}{V_{in}}\right)_{0.6r_{min,i}}}{\left(\frac{V_r}{V_{in}}\right)_{baseline}}$	$\dfrac{\left(\frac{V_\theta}{V_{in}}\right)_{0.6r_{min,i}}}{\left(\frac{V_\theta}{V_{in}}\right)_{baseline}}$
Row 1 entry	0.60	0.70
Row 2 entry	0.57	0.26
Row 3 entry	0.57	0.27
Row 4 entry	0.57	0.25
Row 5 entry	0.57	0.26
Row 5 Exit	0.54	0.34

After analysing the flow behaviour and energy loss in both linear and quick opening trims, and quantifying the effects of the geometrical features of flow paths on Cv_{Trim}, it is essential to find out the root cause for these variations, which can be used in the design phase of the trims. For this purpose, the central gap ratio parameter (d_{i+1}/d_i) for the different trims considered is presented in table 5.

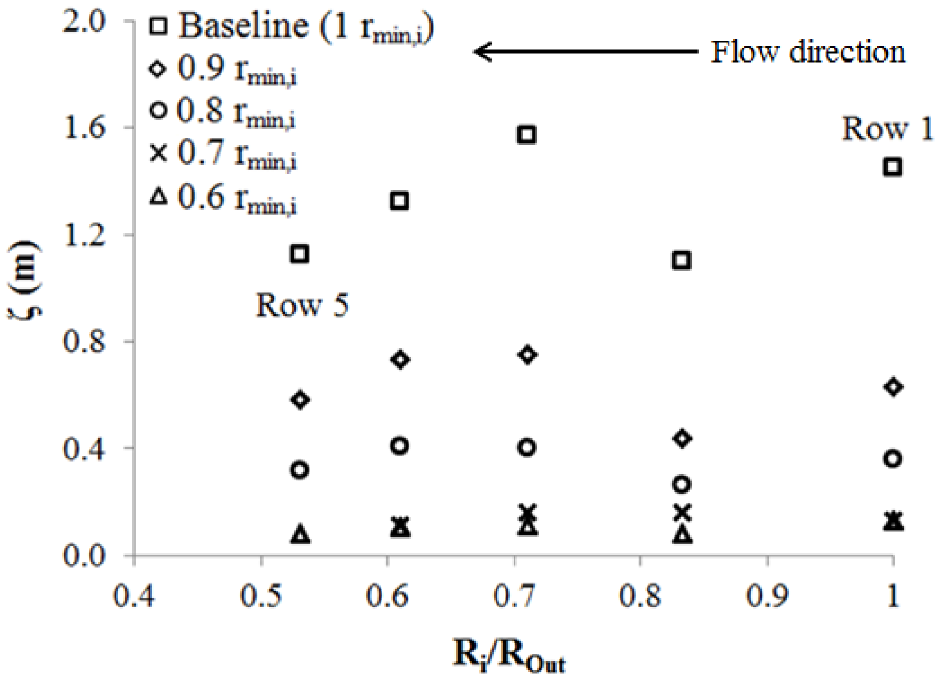

Figure 18 Comparison of energy loss parameter between the linear and quick opening trims

As expected, flow path central gap increases from rows 1 to 2, while it decreases from rows 2 to 3 for all the modified trims (as observed in the baseline trim). From rows 3 to 4, and 4 to 5, it increases again. Moreover, the central gap between the walls of flow paths increases from $0.9r_{min,i}$ to $0.6r_{min,i}$ trims. However, the most interesting observation is the average d_{i+1}/d_i value of these trims. The average central gap ratio parameter for linear opening trims is =>1, while for quick opening trims, it is <1. Hence, the central gap ratio parameter (d_{i+1}/d_i) can be used as a design parameter for the inherent opening characteristics of multi-stage continuous-resistance trims.

Table 5 Variations in d_{i+1}/d_i for different sized flow paths

d_{i+1}/d_i	$0.9r_{min,i}$	$0.8r_{min,i}$	$0.7r_{min,i}$	$0.6r_{min,i}$
d_2/d_1	1.02	0.97	0.93	0.91
d_3/d_2	0.88	0.87	0.87	0.86
d_4/d_3	1.10	1.04	0.99	0.96
d_5/d_4	1.17	1.10	1.05	1.01
Average	1.04	1.00	0.96	0.94

6.0 Flow path manipulation for the recovery of inherent opening characteristics

It has been concluded that $0.6r_{min,i}$ is a quick opening trim in which the energy loss is considerably less. Hence, this particular trim has both one unfavourable (quick opening) and one favourable characteristic (less energy loss). In the present study, flow path manipulation has carried out in order to change this trim's inherent opening characteristic to linear opening, as per the design need, while retaining the less energy loss characteristic. This has been achieved by blocking some of the flow paths of this trim so that flow cannot take place through them. By blocking some flow paths, same flow rate of water has to propagate through reduced area within the trim. This in-turn will regulate hydrodynamic losses within the trim, which may modify the constant energy loss trend within this trim, making it a linear opening trim. At the same time, large central gaps between the walls of flow paths (d_i) are expected to balance out the additional energy loss within the trim to some extent. Hence, in stage 1 of flow path manipulation investigations, half of the flow paths have been blocked. This has been numerically modelled by removing two complete quarters of the trim, from each disc. The resulting geometric configuration of the trim is shown in figure 19. This trim has been referred to as $0.6r_{min,i}$ continuous blocked trim hereafter. It should be note that the right hand side quarter shown in figure 19 is the one that is in-line with the inlet boundary of the flow domain.

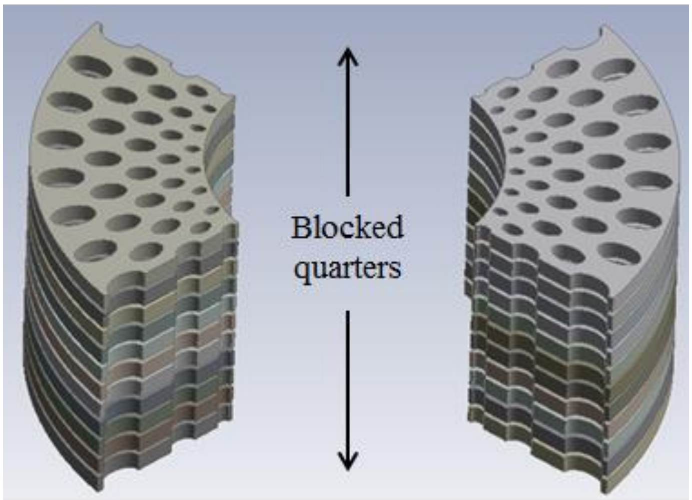

Figure 19 $0.6r_{min,i}$ continuous blocked trim

Figure 20 depicts the variations in non-dimensional pressure and flow velocity magnitude within the top disc of $0.6r_{min,i}$ continuous blocked trim at 100% VOP. It can be seen that there are four sections in the bore region of the trim where non-dimensional pressure is significantly higher than the rest of the trim; hence, static pressure in these sections is very low compared to the static pressure at the inlet of the flow domain. This suggests that there are significant chances of cavitation in these sections. Moreover, non-dimensional pressure at the entry of rows 1 to 5 has been recorded to be 4.5%, 12.1%, 17.7%, 25.1% and 31.1% of the inlet pressure, which is 7.9times, 7.2times, 7.1times, 6.9times and 6.9times greater than $0.6r_{min,i}$ trim respectively. Moreover, the non-dimensional flow velocity magnitude distribution shown in figure 20(b) depicts very high velocity in the sections where lower pressure has been observed. It has been computed that the non-dimensional flow velocity magnitude at the entry of rows 1 to 5 is 2.0times, 2.3times, 2.4times, 2.4times and 2.4times higher in $0.6r_{min,i}$ continuous blocked trim, compared to $0.6r_{min,i}$ trim. These observations ascertain that $0.6r_{min,i}$ continuous blocked trim is unsuitable for commercial viability, and needs major modifications to its design.

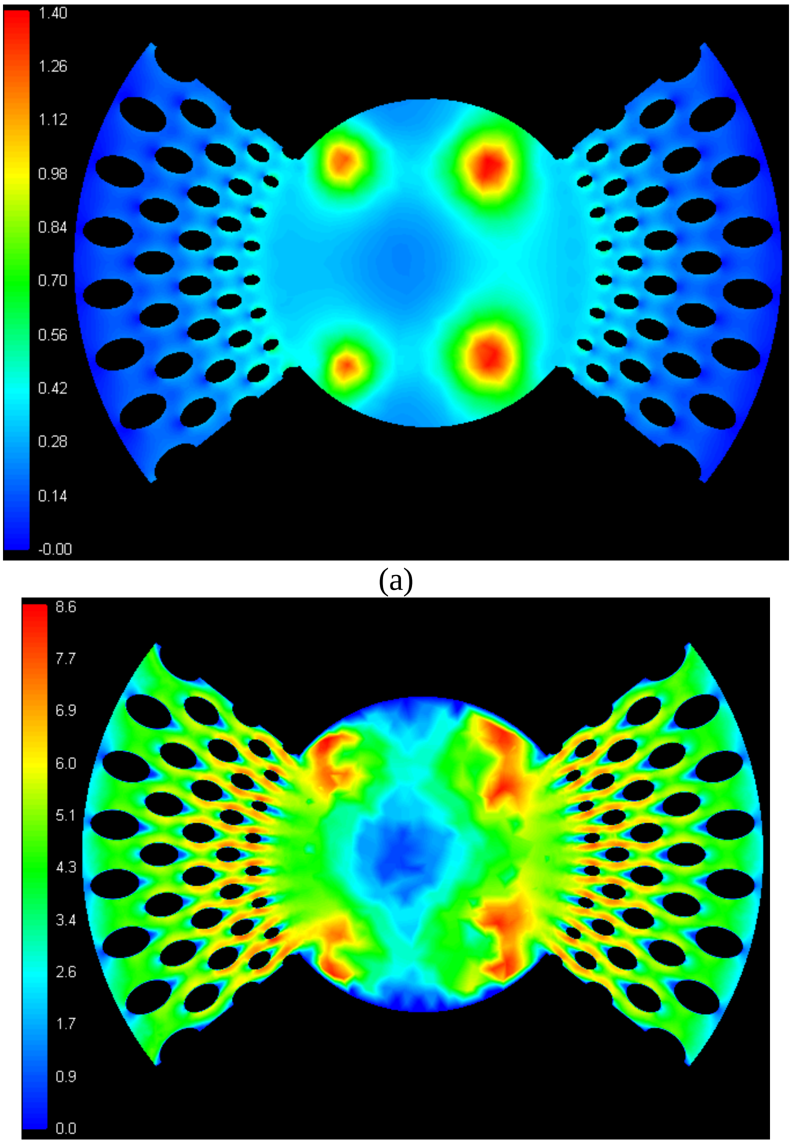

(b)

Figure 20 Variations of (a) non-dimensional pressure and (b) non-dimensional flow velocity magnitude within $0.6r_{min,i}$ continuous blocked trim

Although it has been analysed that $0.6r_{min,i}$ continuous blocked trim is commercially unsuitable due to low pressure zones in the bore region of the trim, it is yet to be analysed whether blocking the flow paths do help in changing/recovering the inherent opening characteristics of a multi-stage continuous-resistance trim. Hence, variations in energy loss parameter (ζ) across the different rows of $0.6r_{min,i}$ continuous blocked trim are shown in figure 21. It can be clearly seen that there are significant variations in ζ in different rows of $0.6r_{min,i}$ continuous blocked trim, indicating that its inherent opening characteristic has changed from quick to linear opening. In comparison with the baseline trim, it can be further noticed that the energy loss in $0.6r_{min,i}$ continuous blocked trim is less. Thus, this trim is now a linear opening trim with less energy loss, but depicts higher flow velocity (meaning more erosion and wear) and lower pressure (cavitation potential), which makes this trim commercially unviable.

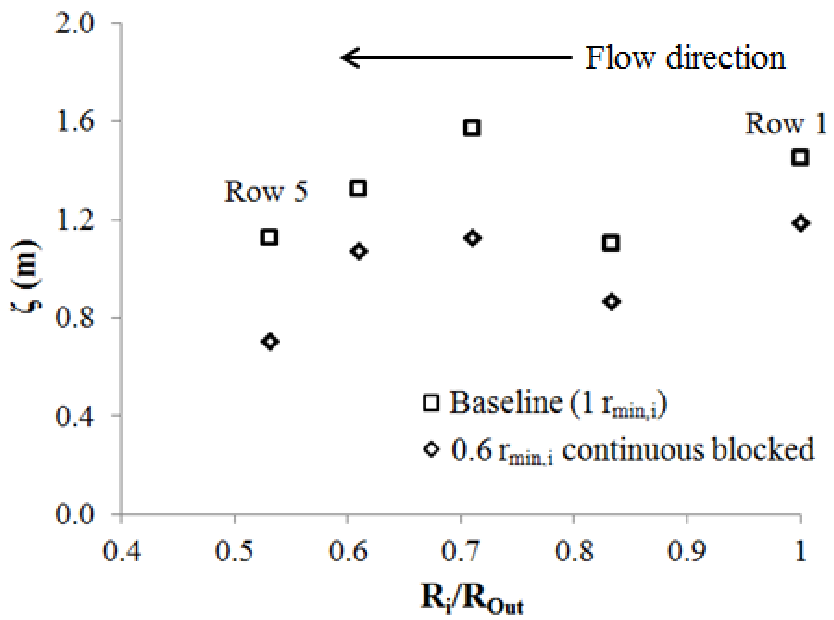

Figure 21 Comparison of energy loss parameter between the baseline and $0.6r_{min,i}$ continuous blocked trims

In order to develop an acceptable trim design with $0.6r_{min,i}$ flow paths and linear opening characteristics, the root cause for low pressure sections in the bore region of $0.6r_{min,i}$ continuous blocked trim must be found. It has been observed in figure 20 that the low pressure sections in the trim are areas of recirculating flow. Jets of flow exiting the flow paths of either quarters of the trim meet in the bore region. In case of unblocked trims, flow jets were emerging from the flow paths of all the four quarters of the trim, resulting in complex flow interactions/mixing, which avoids the formation of recirculation zones. Flow mixing is also possible in blocked trims by careful manipulation of blocked flow paths, and the desired results may be achieved. Hence, in stage 2 of this investigation, instead of blocking all the flow paths of the same two quarters throughout the trim, an alternative blocking configuration has been developed. In this blocking configuration, flow paths of the same two quarters have been blocked (in disc 1 only) as in case of $0.6r_{min,i}$ continuous blocked trim. However, in disc 2 of the trim, the flow paths of these two quarters are now open, while the flow paths of the other two quarters have been blocked. Hence, discs 1, 3, 5, 7, 9 and 11 are identical in blocking pattern, while discs 2, 4, 6, 8 and 10 are identical. This trim has been referred to as $0.6r_{min,i}$ alternative blocked trim hereafter, and has been shown in figure 22 (also shown in figure 25).

Analysing the flow behaviour in $0.6r_{min,i}$ alternative blocked trim, it can be seen in figure 23(a) that the scale of non-dimensional pressure variations is comparable to the baseline trim (in figure 10), and is significantly lower than that for $0.6r_{min,i}$ continuous blocked trim. The non-dimensional pressure increases systematically from row 1 to 5, indicating loss in static pressure. The higher non-dimensional pressure field in the bore region of this trim also resembles in scale and distribution to the one observed in case of the baseline trim. Hence, the low pressure regions no longer exist. Moreover, the non-dimensional flow velocity magnitude in figure 23(b) shows that no recirculation zones are present in the bore region of the trim. These results indicate that $0.6r_{min,i}$ alternative blocked trim design is suitable for commercial viability.

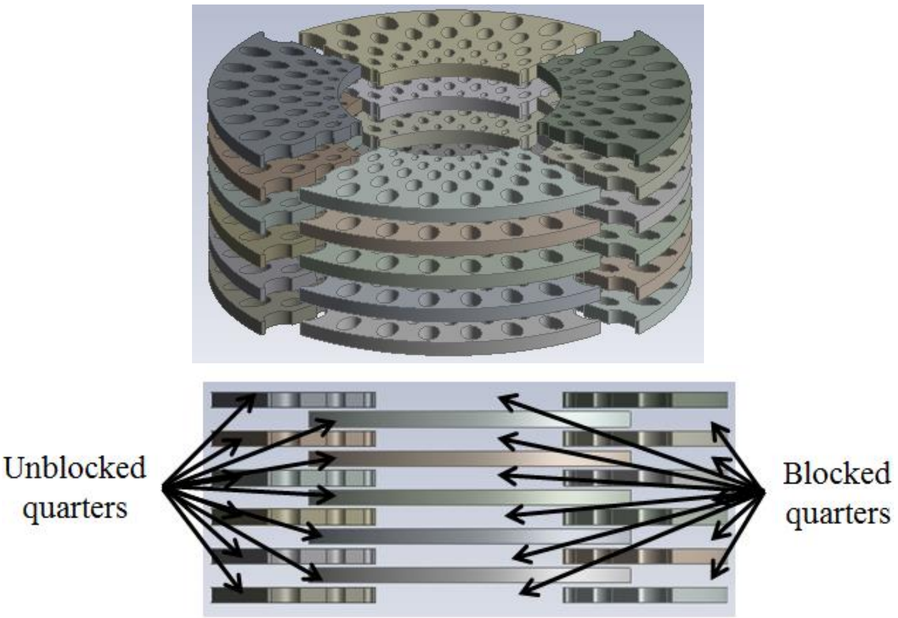

Figure 22 $0.6r_{min,i}$ alternative blocked trim

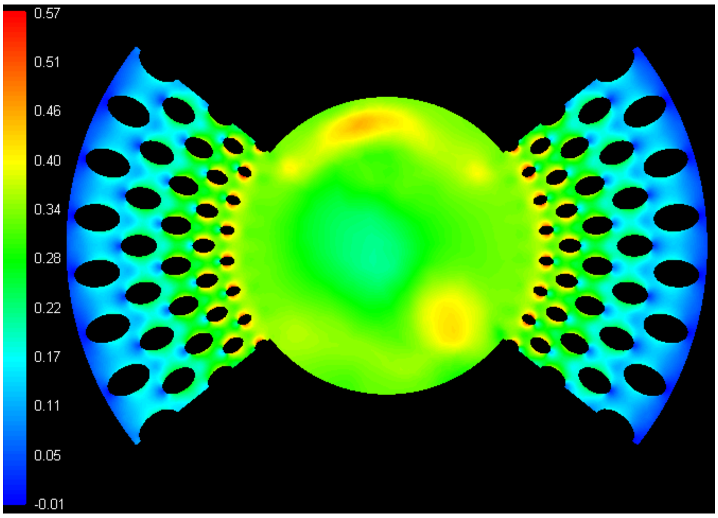

(a)

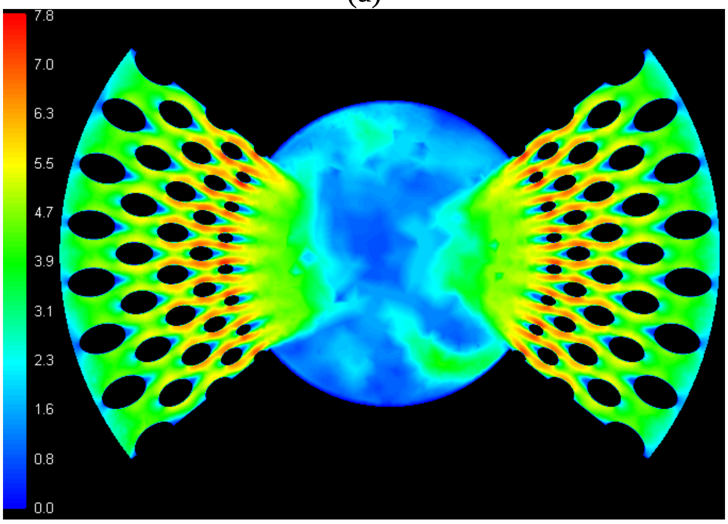

(b)

Figure 23 Variations of (a) non-dimensional pressure and (b) non-dimensional flow velocity magnitude within $0.6r_{min,i}$ continuous blocked trims

Confirming whether 0.6$r_{min,i}$ alternative blocked trim is a linear opening trim, variations in the energy loss parameter (ζ) across the different rows of this trim have been depicted in figure 24. It can be clearly seen that the trends in energy loss resembles the one observed in case of linear opening trims. Moreover, in comparison with both the baseline and 0.6$r_{min,i}$ continuous blocked trims, it can be noticed that energy loss across the different rows of 0.6$r_{min,i}$ alternative blocked trim is less than both these trims. The energy loss across rows 1 to 5 of 0.6$r_{min,i}$ alternative blocked trim is 22.2%, 33.5%, 34.4%, 31.0% and 42.0% less than the baseline trim. Hence, 0.6$r_{min,i}$ alternative blocked trim is more energy efficient than the baseline trim, and is suitable for commercial applications.

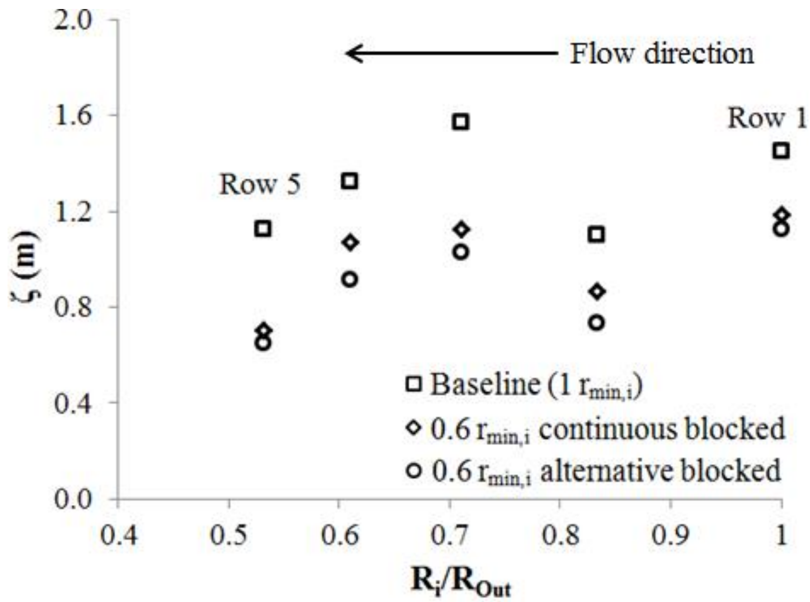

Figure 24 Comparison of energy loss parameter between the baseline and the blocked trims

Based on the numerically predicted results, it has been concluded that 0.6$r_{min,i}$ alternative blocked trim is an energy efficient linear opening trim. In order to prove this concept, and to validate the numerical predictions, 0.6$r_{min,i}$ alternative blocked trim has been manufactured for experimental testing, as shown in figure 25. This trim has been extensively tested in the flow loop using standard experimental procedures discussed in section 2 of this study. Based on the differential pressure and flow rate measurements across the control valve installed with 0.6$r_{min,i}$ alternative blocked trim, Cv_{Trim} values at various valve opening positions have been computed.

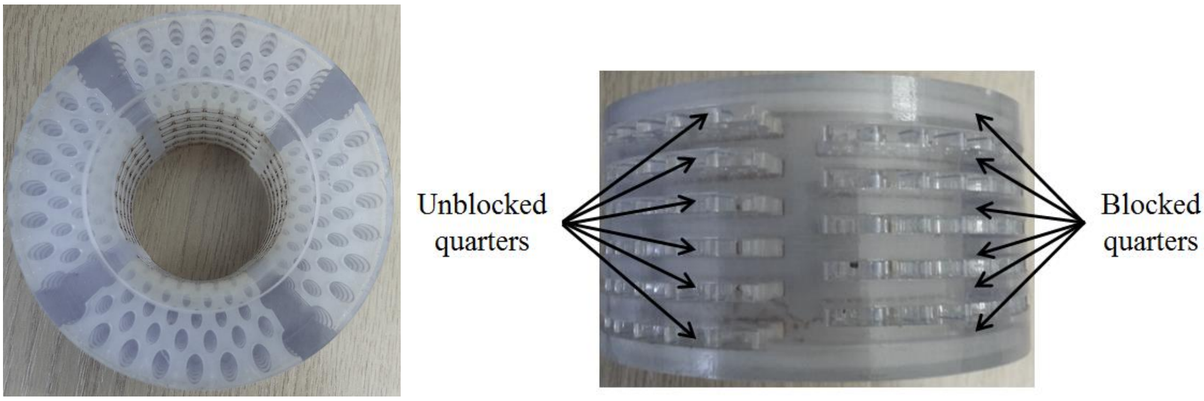

Figure 25 0.6$r_{min,i}$ alternative blocked trim

It can be seen in figure 26 that $0.6r_{min,i}$ alternative blocked trim is indeed a linear opening trim. The numerically predicted results match closely with the experimental measurements, at all different valve opening positions considered. The average difference between the two results has been calculated to be 3.3%. Hence, it can be concluded, based on the results presented in this study, that $0.6r_{min,i}$ alternative blocked trim is commercially more viable than the baseline trim as it exhibits less energy loss. The manufacturing cost of this trim is less than the baseline trim as half of the flow paths are blocked, and hence, $0.6r_{min,i}$ alternative blocked trim is more cost effective as well.

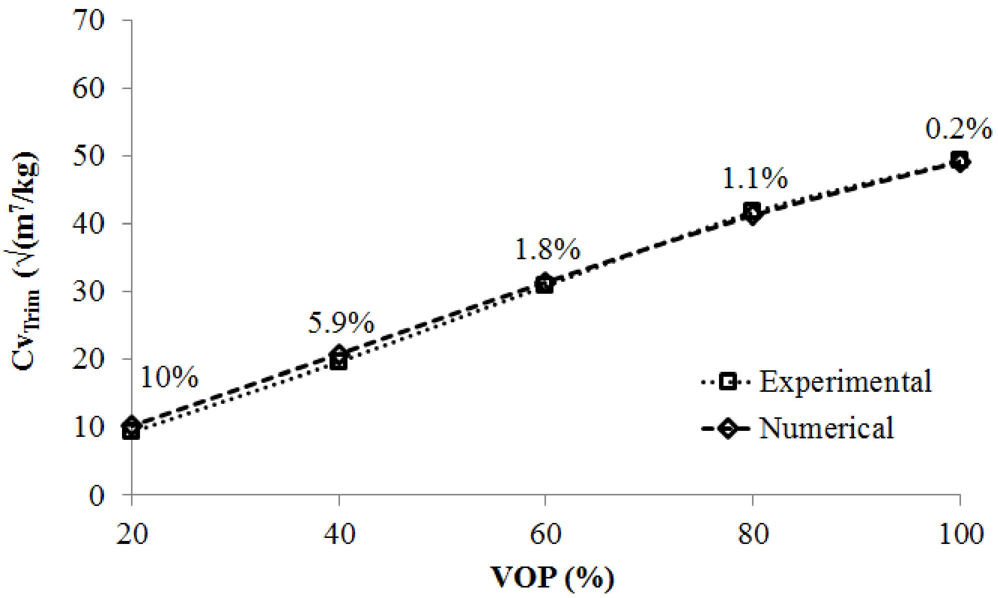

Figure 26 Comparison of numerical and experimental Cv_{Trim} of $0.6r_{min,i}$ alternative blocked trim

7.0 Conclusions

Control valves are extensively used in a variety of different energy systems. The flow within the control valves is managed by multi-stage continuous-resistance trims. The flow capacity of these trims depends on the geometrical features of flow paths in these trims. In the present study, detailed numerical investigations have been carried out to analyse these effects using a commercial Computational Fluid Dynamics based solver. The numerical predictions have been compared against the experimental results wherever possible to ascertain the accuracy of the numerical results. It can be concluded from the results presented in this study that the geometrical features of flow paths in multi-stage continuous-resistance trims significantly affect the flow capacity of the trims. It has been shown that by reducing the gap between the walls of flow paths (d_i), the flow capacity of the trim increases. Reduction in d_i increases the area available for the flow to take place, hence reducing the resistance to flow, which in-turn reduces the energy loss across the trim. It has been further noticed that at a critical central gap width ($0.7\ r_{min,i}$), the inherent opening characteristics of the trim changes. This is accompanied with a constant energy loss across the different rows of the trim. Change in the inherent opening characteristics of a multi-stage continuous-resistance trim is that the central gap ratio parameter drops below 1. Upon careful manipulation of flow paths, the inherent opening characteristics of the trim can be recovered, while still having lower energy loss across the trim. This flow path manipulation is associated with a systematic blocking of a certain number of flow paths. It has been shown that alternative blocking of flow paths results in an improved trim design that is both cost effective and commercially viable.

Nomenclature

Cv	Flow capacity (($\sqrt{m^7/kg}$))
Cv_{Seat}	Flow capacity of the seat ($\sqrt{m^7/kg}$)
Cv_{Body}	Flow capacity of the valve body ($\sqrt{m^7/kg}$)
Cv_{Trim}	Flow capacity of the trim ($\sqrt{m^7/kg}$)
Cv_{Valve}	Flow capacity of the control valve ($\sqrt{m^7/kg}$)
d_i	Central distance between the walls of flow paths of the i^{th} row (m)
D	Diameter of pipeline (m)
g	Gravitational Acceleration (m/s^2)
p	Local static pressure (kPa)
p_i	Average static pressure upstream the i^{th} row (kPa)
P_{in}	Static pressure at the inlet of the flow domain (kPa)
ΔP	Differential pressure (kPa)
Q	Volumetric flow rate (m^3/hr)
$r_{min,i}$	Minor radius of curvature of flow paths' walls of the i^{th} row (m)
$r_{max,i}$	Major radius of curvature of flow paths' walls of the i^{th} row (m)
R_i	Radius at the entry/exit of i^{th} row of the trim (m)
R_{out}	Outer radius of the trim (m)
v	Flow velocity magnitude (m/s)
v_r	Radial flow velocity component (m/s)
v_θ	Tangential flow velocity component (m/s)
v_z	Axial flow velocity component (m/s)
V_i	Average flow velocity magnitude upstream the i^{th} row (m/s)
V_{in}	Flow velocity magnitude at the inlet of the flow domain (m/s)

Greek Symbols

β	Numerical constant (-)
γ	Piping geometry factor (-)
ζ	Energy loss parameter (m)
η	Reynolds number factor (-)
k	Turbulent kinetic energy (m^2/s^2)
ρ	Density of the fluid (kg/m^3)
ρ_o	Operating of water (kg/m^3)
ω	Turbulent dissipation rate (1/s)

Abbreviations

CFD	Computational Fluid Dynamics
EDM	Electric Discharge Machining
SLM	Selective Laser Melting
POD	Proper Orthogonal Decomposition
RANS	Reynolds averaged Navier-Stokes
RHS	Right Hand Side
SST	Shear Stress Transport
VOP	Valve Opening Position

References

[1] Industrial process control valves, Part 1: Control valve terminology and general considerations, BS EN 60534-1:2005, British Standards BSI.

[2] Industrial process control valves, Part 2-1: Flow capacity – Sizing equations for fluid flow under installed conditions, BS EN 60534-2-1:2011, British Standards BSI.

[3] K. Morton (2003) Optimisation of a high-energy loss control valve trim using computational and experimental techniques, PhD Thesis, University of Manchester, UK.

[4] E. W. Singleton (2013) A specifier's guide to Control Valves.

[5] J. Green, R. Mishra, M. Charlton and R. Owen (2012) Validation of CFD predictions using process data obtained from flow through an industrial control valve, Journal of Physics: Conference Series (364).

[6] J. Green, R. Mishra, M. Charlton and R. Owen (2012) Local Analysis of Flow Conditions within a Geometrically Complex Control Valve Trim using CFD, Journal of Physics: Conference Series (364).

[7] T. Asim (2013) Capacity testing of X-Stream valves for single-component single-phase flows, Technical report submitted to Weir Valves and Controls Ltd.

[8] M. Charlton (2014) Cost Effective Manufacturing and Optimal Design of X-Stream Trims for Severe Service Control Valves, Masters by Research Thesis, University of Huddersfield, UK.

[9] M. Charlton, R. Mishra and T. Asim (2016) The effect of manufacturing method induced roughness on severe service control valve performance, 43rd National Conference on Fluid Mechanics and Fluid Power, 15-17 December, Allahabad, India.

[10] T. Asim, R. Mishra, M. Charlton and C. Oliveira (2015) Capacity Testing and Local Flow Analysis of a Geometrically Complex Trim Installed within a Commercial Control Valve, International Conference on Jets, Wakes and Separated Flows, 16-18 June, Stockholm, Sweden.

[11] E. Lisowski and G. Filo (2016) CFD analysis of the characteristics of a proportional flow control valve with an innovative opening shape, Energy Conversion and Management (123) 15-28.

[12] X. Zhou, Z. Wang and Y. Zhang (2017) A simple method for high-precision evaluation of valve flow coefficient by computational fluid dynamics simulation, Advances in Mechanical Engineering (9) 1-7.

[13] X. Sun, H. S. Kim, S. D. Yang, C. K. Kim and J. Y. Yoon (2017) Numerical investigation of the effect of surface roughness on the flow coefficient of an eccentric butterfly valve, Journal of Mechanical Science and Technology (31) 2839-2848.

[14] T. Asim, M. Charlton and R. Mishra (2017) CFD based Investigations for the Design of control Valves used in Energy Systems, Energy Conversion and Management (153) 288-303.

[15] A. Oliveira (2017) Capacity testing of X-Stream valves for single-component single-phase flows, Technical report submitted to Weir Valves and Controls Ltd

[16] L. Kong, W. Wei and Q. Yan (2018) Application of flow field decomposition and reconstruction in studying and modeling the characteristics of a cartridge valve, Engineering Applications of Computational Fluid Mechanics (12) 385-396.

[17] Industrial process control valves, Part 2-4: Flow capacity – Inherent flow characteristics and rangeability, BS EN 60534-2-4:2003, British Standards BSI.

[18] Industrial process control valves, Part 2-5: Flow capacity – Sizing equations for fluid flow through multistage control valves with interstage recovery, BS EN 60534-2-5:2009, British Standards BSI.

[19] Industrial process control valves, Part 2-3: Flow capacity – Test procedures, BS EN 60534-2-3:1998, British Standards BSI.

[20] T. Asim, A. Algadi and R. Mishra (2018) Effect of capsule shape on hydrodynamic characteristics and optimal design of hydraulic capsule pipelines, Journal of Petroleum Science and Engineering (161) 390-408.
[21] T. Asim and R. Mishra (2016) Computational Fluid Dynamics based Optimal Design of Hydraulic Capsule Pipelines Transporting Cylindrical Capsules, International Journal of Powder Technology (295) 180-201.
[22] T. Asim, R. Mishra, S. Abushaala and A. Jain (2016) Development of a Design Methodology for Hydraulic Pipelines carrying Rectangular Capsules; International Journal of Pressure Vessels and Piping (146) 111-128.
[23] T. Asim and R. Mishra (2016) Optimal Design of Hydraulic Capsule Pipelines Transporting Spherical Capsules, The Canadian Journal of Chemical Engineering (94) 966-979.
[24] V. Malviya, T. Asim, I. Sendanayake and R. Mishra (2018) Development of a Novel Characterisation Methodology for the Aerodynamic Coefficients of a Tractor–Trailer Unit Based on Relative Flow Angles and Vehicle Dimensions; Arabian Journal for Science and Engineering 1-19.
[25] T. Asim and R. Mishra (2017) Large Eddy Simulation based Analysis of Complex Flow Structures within the Volute of a Vaneless Centrifugal Pump, Sadhana (42) 505-516.
[26] Ansys 17.0 User Guide available online.
[27] T. Asim, R. Mishra, L. E. Kollar and S. R. Pradhan (2013) Optimal Sizing and Life-Cycle Cost Modelling of Pipelines Transporting Multi-Sized Solid-Liquid Mixtures, International Journal of Pressure Vessels and Piping (113) 40-48.
[28] S. Pradhan, R. Mishra, K. Ubbi and T. Asim (2013) Optimal Design of a Four-Sensor Probe System to Measure the Flow Properties of the Dispersed Phase in Bubbly Air-Water Multiphase Flows, Sensors and Actuators A:Physical (201) 10-22.
[29] F. R. Menter (1994) Two-Equation Eddy-Viscosity Turbulence Models for Engineering Applications, American Institute of Aeronautics and Astronautics (32) 1598-1605.
[30] E. Palmer, R, Mishra and J. Fieldhouse (2008) A computational fluid dynamic analysis on the effect of front row pin geometry on the aerothermodynamic properties of a pin-vented brake disc, Proceedings of the Institution of Mechanical Engineers Part D: Journal of Automobile Engineering (222) 1231-1245.
[31] A. Shahzad, T. Asim, R. Mishra and A. Paris (2013) Performance of a Vertical Axis Wind Turbine under Accelerating and Decelerating Flows, Procedia CIRP: 2nd International Through-life Engineering Services Conference (11) 311-316.
[32] K. Park, T. Asimand R. Mishra (2012) Computational Fluid Dynamics based Fault Simulations of a Vertical Axis Wind Turbines, Journal of Physics: Conference Series (364) 012138.
[33] B. Tesfa, F. Gu, R. Mishra and A. Ball (2013) LHV predication models and LHV effect on the performance of CI engine running with biodiesel blends, Energy Conversion and Management (71) 217-226.
[34] H. K. Versteeg and W. Malalasekera (1995) An Introduction to Computational Fluid Dynamics, Longman Scientific and Technical, U.K. ISBN: 0131274988.
[35] S. V. Patankar and D. B. Spalding (1972) A Calculation Procedure for Heat, Mass and Momentum Transfer in Three-Dimensional Parabolic Flows, Heat and Mass Transfer (15) 1787-1806.
[36] V. C. Agarwal and R. Mishra (1998) Optimal design of a multi-stage capsule handling multi-phase pipeline, International Journal of Pressure Vessels and Piping (75) 27-35.